Dual functional states of R406W-desmin assembly complexes cause cardiomyopathy with severe intercalated disc derangement in humans and in knock-in mice

Harald Herrmann, Eva Cabet, Nicolas Chevalier, Julia Moosmann, Dorothea Schultheis, Jan Haas, Mirjam Schowalter, Carolin Berwanger, Veronika Weyerer, Abbas Agaimy, et al.

Dual functional states of R406W-desmin assembly complexes cause cardiomyopathy with severe intercalated disc derangement in humans and in knock-in mice

Harald Herrmann, PhD[1,2,*,#], Eva Cabet, PhD[3,*], Nicolas R. Chevalier, PhD[4], Julia Moosmann, MD[5], Dorothea Schultheis, PhD[1], Jan Haas, PhD[6], Mirjam Schowalter[1], Carolin Berwanger[7], Veronika Weyerer, MD[8], Abbas Agaimy, MD[8], Benjamin Meder, MD[6,9], Oliver J. Müller, MD[10], Hugo A. Katus, MD[11], Ursula Schlötzer-Schrehardt, PhD[12], Patrick Vicart, PhD[3], Ana Ferreiro, MD[3,13], Sven Dittrich, MD[5], Christoph S. Clemen, MD[7,14,15,§], Alain Lilienbaum, PhD[3,§,#], Rolf Schröder, MD[1,§,#]

1 Institute of Neuropathology, University Hospital Erlangen, Friedrich-Alexander University Erlangen-Nürnberg, Erlangen, Germany
2 B060 - Molecular Genetics, German Cancer Research Center, Heidelberg, Germany
3 Basic and Translational Myology, Unit of Functional and Adaptive Biology, Université de Paris / CNRS UMR 8251, Paris, France
4 Laboratoire Matière et Systèmes Complexes, Université de Paris / CNRS UMR 7057, Paris, France
5 Department Pediatric Cardiology, University Hospital Erlangen, Friedrich-Alexander University Erlangen-Nürnberg, Erlangen, Germany
6 Institute for Cardiomyopathies Heidelberg, Heart Center Heidelberg, University of Heidelberg, Heidelberg, Germany
7 Institute of Aerospace Medicine, German Aerospace Center, Linder Höhe, Cologne, Germany
8 Institute of Pathology, University Hospital Erlangen, Friedrich-Alexander University Erlangen-Nürnberg, Erlangen, Germany
9 Stanford University School of Medicine, Department of Genetics, Stanford, California, USA
10 Internal Medicine III, University Hospital Schleswig-Holstein and University of Kiel, Kiel, and DZHK (German Center for Cardiovascular Research), Partner site Hamburg/Kiel/Lübeck, Kiel, Germany
11 Department of Cardiology, Medical University Hospital Heidelberg, and German Center for Cardiovascular Research, Partner site Heidelberg/Mannheim, Heidelberg, Germany
12 Department of Ophthalmology, University Hospital Erlangen, Friedrich-Alexander University Erlangen-Nürnberg, Erlangen, Germany
13 AP-HP, Reference Center for Neuromuscular Disorders, Pitié-Salpêtrière Hospital, Paris, France
14 Center for Physiology and Pathophysiology, Institute of Vegetative Physiology, Medical Faculty, University of Cologne, Cologne, Germany
15 Center for Biochemistry, Institute of Biochemistry I, Medical Faculty, University of Cologne, Cologne, Germany

*These first authors contributed equally to this work.

§These senior authors contributed equally to this work.

Running title: R406Wdesmin causes cardiomyopathy in humans & mice

#Authors for correspondence:

Harald Herrmann, Institute of Neuropathology, University Hospital Erlangen, Schwabachanlage 6, 91054 Erlangen, Germany; Phone: +49 9131 85 44579; h.herrmann@dkfz-heidelberg.de;

Alain Lilienbaum, Fundamental and Translational Myology Laboratory, Unit of Functional and Adaptive Biology / CNRS UMR8251, Université de Paris, 5 rue Lagroua-Weill Hallé, 75013 Paris, France; Phone: +33 1 57277965; alain.lilienbaum@u-paris.fr

Rolf Schröder, Institute of Neuropathology, University Hospital Erlangen, Schwabachanlage 6, 91054 Erlangen, Germany; Phone: +49 9131 85 34782; rolf.schroeder@uk-erlangen.de

Abstract

Background: Mutations in the human desmin gene cause myopathies and cardiomyopathies. Aim of this study was to elucidate molecular mechanisms initiated by the heterozygous R406W-desmin mutation in the development of a severe and early-onset cardiac phenotype.

Methods: We report an adolescent patient, who underwent cardiac transplantation due to restrictive cardiomyopathy caused by a heterozygous R406W-desmin mutation. Sections of the explanted heart were analyzed with antibodies specific to 406W-desmin and to intercalated disc proteins. Effects of the R406W mutation on the molecular properties of desmin were addressed by cell transfection and *in vitro* assembly experiments. To prove the genuine deleterious impact of the mutation on heart tissue, we further generated and analyzed R405W-desmin knock-in mice harboring the orthologous form of the human R406W-desmin.

Results: Microscopic analysis of the explanted heart revealed desmin aggregates and the absence of desmin filaments at intercalated discs. Structural changes within intercalated discs were revealed by the abnormal organization of desmoplakin, plectin, N-cadherin, and connexin-43. Next generation sequencing confirmed the *DES* variant c.1216C>T (p.R406W) as the sole disease-causing mutation. Cell transfection studies disclosed a dual behavior of R406W-desmin with both its integration into the endogenous intermediate filament system and segregation into protein aggregates. *In vitro*, R406W-desmin formed unusually thick filaments that organized into complex filament aggregates and fibrillar sheets. In contrast, assembly of equimolar mixtures of mutant and wild-type desmin generated chimeric filaments of seemingly normal morphology but with occasional prominent irregularities. Heterozygous and homozygous R405W-desmin knock-in mice develop both a myopathy and a cardiomyopathy. In particular, the main histopathological results from the patient are recapitulated in the hearts from R405W-desmin knock-in mice of both genotypes. Moreover, while heterozygous knock-in mice have a normal life span, homozygous animals die at three months of age due to a smooth muscle-related gastrointestinal phenotype.

Conclusions: We demonstrate that R406W-desmin provokes its severe cardiotoxic potential by a novel pathomechanism, where the concurrent dual functional states of mutant desmin assembly complexes underlie the uncoupling of desmin filaments from intercalated discs and their structural disorganization.

Keywords

intermediate filaments; desmin; desminopathy; cardiomyopathy; intercalated disc; desmosome; striated muscle; smooth muscle; intestinal pseudo-obstruction

Clinical perspective

What is new?

- We demonstrate a novel pathomechanism in which cardiotoxic R406W-desmin can adopt dual functional states with the abilities to integrate into the endogenous intermediate filament network and to cause formation of protein aggregates.

- R406W-desmin modifies the extra-sarcomeric cytoskeleton such that desmin filaments are not anchored to desmosomes anymore, thereby destroying the structural and functional integrity of intercalated discs.

- The observed disorganization of the extra-sarcomeric cytoskeleton itself in conjunction with the compromised attachment of desmin filaments to cardiac desmosomes is the structural and functional basis for the early development of cardiac disease manifestation rather than the presence of “toxic” R406W-desmin aggregates.

What are the clinical implications?

- Certain heterozygous *DES* mutation carriers will develop early-onset progressive cardiomyopathy necessitating cardiac transplantation within a few years after disease onset.

- Since “cardiotoxic” desmin mutations can affect the integrity of intercalated discs thereby inducing conduction defects and malignant arrhythmias, early implantation of pacemaker/cardioverter defibrillator devices is highly justified to prevent sudden cardiac death.

- State-of-the-art basic molecular risk stratification of desmin mutations should encompass a multi-disciplinary experimental approach comprising assessment of the tissue pathology in conjunction with genome analysis and desmin assembly studies; however, for the *in vivo* validation of desmin mutations, patient-mimicking cell and animal models are still indispensable.

Introduction

Desmin is a fibrous protein of 470 amino acids that belongs to the intermediate filament multi-protein family. The protein is abundantly expressed in cardiac and skeletal muscle of vertebrates. There, desmin forms extended filaments that act as an essential structural and functional component of the three-dimensional extra-sarcomeric cytoskeleton [1]. The filamentous network exerts multiple roles in the alignment and anchorage of myofibrils, the positioning of mitochondria and myonuclei, mechanosensing, and stress tolerance [1-3]. In the heart, desmin is prominently present at the level of myofibrillar Z-discs and intercalated discs. Through its attachment to various intracellular adhesion sites mediated by a group of high-molecular weight cross-bridging factors of the spectrin superfamily such as desmoplakin, plectin, nebulin, nebulette, and nesprin, the desmin system forms a complex composite network designed to buffer mechanical stress imposed on the myocyte [1, 3]. Thereby desmin is acting as a mechanochemical integrator that structurally and functionally links the extracellular matrix to cellular organelles including the nucleus [4]. Desmin is, together with many of the above listed associated proteins, highly conserved in vertebrate evolution, indicating it is indeed a basic functional component of muscle.

For the human desmin gene (*DES*) a multitude of inherited mutations have been described ([1, 3]; Human Intermediate Filament Database, www.interfil.org). In addition to autosomal-dominant cases, which represent the most frequent form, a growing number of sporadic and autosomal-recessive cases have been reported. The many different amino acids changes cause a broad spectrum of familial and sporadic cardiomyopathies and myopathies referred to as “desminopathies”, with disease onsets ranging from the first to the eighth decade of life [1]. Desminopathies can manifest with pure cardiomyopathy, myopathy, or both combined. Cardiac disease manifestations comprising true cardiomyopathy as well as various forms of cardiac conduction defects and arrhythmia may precede, coincide with, or succeed skeletal muscle involvement [1, 5]. The major causes of premature mortality in desminopathies are sudden cardiac death and progressive heart failure [1, 3, 5]. The clinically more severe recessive cases due to homozygous or compound heterozygous *DES* mutations can be subdivided into a group with complete lack of desmin [6-9] and two groups with sole expression of a mutant desmin either without [10] or with [11-15] protein aggregate formation.

In the present study, we unravel the deleterious functional characteristics of the heterozygous *DES* mutation c.1216C>T (p.R406W), which we identified as the causative gene defect in an adolescent male patient with progressive restrictive cardiomyopathy, cardiac conduction defects, and arrhythmias. This young man, like all of the few up to now reported patients carrying this mutation, had an early disease onset and severe cardiac disease, which argues that arginine 406 to tryptophan is a particularly harmful desmin mutation (for review see [1, 3]). We demonstrate that this mutation compromises desmin filament attachment to intercalated discs. In transfection and assembly studies, we delineate a novel, dual assembly property of the mutant desmin. The mutant protein forms, at least in part, complexes that are able to properly integrate into wild-type desmin filaments thus introducing segments into the filaments that are prone to aggregate upon being mechanically stressed. In order to investigate the impact of the mutant protein on the function of muscle cells and tissues, we generated the R405W-desmin knock-in mouse model harboring the human R406W-desmin ortholog. These mice develop a cardiomyopathy and myopathy exhibiting desmin-positive protein aggregates that are the typical pathomorphological phenotype in desminopathies. Unexpectedly, homozygous mice die at three months of age due to a smooth muscle-related gastrointestinal pseudo-obstruction, which is not encountered in heterozygous mice. In summary, our detailed analysis of the cardiac pathology in the patient and in R405W-desmin knock-in mice highlights the deleterious effect of R405W-desmin on the structural integrity of intercalated discs.

Materials and Methods

For complete and detailed information on clinical investigations, routine histology, generation of R405W-desmin knock-in mice, cardiac echography of mice, intestinal force measurement of mice, transient and stable desmin transfection studies, generation of rabbit polyclonal antibodies for detection of total desmin (wild-type and mutant) as well as human R406W- and murine R405W-desmin, other primary and secondary antibodies, immunofluorescence microscopy, protein biochemical procedures, immunoblotting, transmission electron microscopy, and statistical analyses please refer to the Expanded Materials and Methods section.

The authors declare that all supporting data are available within the article. In case, further data that support the findings of this study will be needed they are available from the corresponding authors on reasonable request.

Editorial Policies and Ethical Considerations

Informed consent in writing was obtained from the reported patient. Consultation with the local Ethics committee clarified that the use of the tissue specimens of the patient's explanted heart does not require special approval when used for a single case description. Regarding the cardiac tissue specimens from an anonymous autopsy case used for control, the local Ethics committee stated (reference number 28_19 Bc) that this is in keeping with the German legal regulations.

Generation and genotyping of R405W-desmin knock-in mice

The R405W-desmin knock-in mouse model C57BL/6N-*Des*$^{tm1.1Allb}$ (http://www.informatics.jax.org/allele/MGI:6382607) was generated according to our specifications (AL) by the Center for Immunophenomics, Marseille, France. Mice were handled in accordance with European Union guidelines and French regulations for animal experimentation, and the investigations were approved by the University Paris Diderot local committee (authorization number CEB-16-2016 / 2016041216476300).

Statistical analysis

For statistical evaluation the non-parametric test function “nparcomp” of the free software R was used with Dunnet comparison to wild-type, Tukey comparison for others, or the Kruskal-Wallis test. Differences were considered significant with $p<0.05$.

Results

A rapidly progressing desmin-related restrictive cardiomyopathy necessitating heart transplantation

We report a Caucasian male patient, who in October 2013 presented with episodes of dizziness and near syncope at the age of 15. The initial physical examination at that time revealed generalized skin pallor, mild hepatomegaly, moderate pleural effusions, and moderate ascites. Apart from Crohn's disease, which had been diagnosed in January 2013, his past medical history was uneventful and his family history was negative for cardiac, neuromuscular, and skin diseases. Electrocardiogram on admission showed a first degree and intermittent third degree atrioventricular and bifascicular bundle branch block. Levels of cardiac enzymes including troponin and creatine kinase were normal but brain natriuretic peptide was elevated up to 520 pg/ml (reference value <100 pg/ml).

Subsequent echocardiography and cardiac catheterization disclosed moderate pattern of restrictive cardiomyopathy (pulmonary artery pressure 37/14(24) mmHg (reference value 20/10(15) mmHg), pulmonary capillary wedge pressure 15-21 mmHg (reference values 4-12 mmHg), right ventricular pressure 36/0/4 mmHg (reference values 20/0/4 mmHg), and cardiac index 2 l/min/m^2 (reference value 2.5-4 l/min/m^2)). Cardiac magnetic resonance imaging (Figure 1A,B) identified late gadolinium-enhancement especially in basal (anterior and inferolateral) and medial (anteroseptal, anterolateral) segments with mild myocardial edema. A first diagnostic cardiac biopsy displayed increased interstitial connective tissue and signs of a macrophage-dominated chronic myocarditis. However, extensive serological and microbiological diagnostic work-up did not reveal active or persistent myocarditis. Subsequently, the patient received a DDD-pacemaker and was started on enalapril, eplerenone, and torasemide. In December 2013, electrocardiograms documented recurrent episodes of supraventricular and ventricular tachycardia. In May 2014, a second cardiac catheterization showed marked restrictive cardiomyopathy and pulmonary hypertension.

A second cardiac biopsy displayed chronic myocardial pathology with diffuse cardiac fibrosis without inflammation (Figure 1C,D). In June 2014, the patient was listed for heart transplantation. In the same year, Sanger sequencing revealed a heterozygous

missense mutation (c.1216C>T) in exon 6 of *DES*, which leads to the exchange of arginine to tryptophan in codon 406 (p.R406W). This previously reported cardiomyopathy-causing desmin mutation was not detected in his parents suggesting a *de novo* mutation. Biventricular restriction pathology further deteriorated over time leading to progressive heart failure. Since arrhythmias including ventricular tachycardia and atrial fibrillation became more apparent, he was provided with an implantable cardioverter defibrillator system in October 2014. Neurological examination did not show any evidence of skeletal muscle weakness or wasting. He successfully received a heart transplantation in August 2017.

In 2019, we subjected DNA samples of the patient and his parents to targeted next generation sequencing for a comprehensive screen of all relevant genes previously associated with cardiomyopathies. When using stringent filtering for truncating and missense variants on population allele frequency (AF gnomAD exome <0.001), we detected, in addition to the heterozygous *DES* mutation, a further heterozygous variant in the reported patient, which is also shared by his asymptomatic father. This p.Asn761Ser vinculin variant is absent in gnomAD and can be classified as “uncertain significance” according to American College of Medical Genetics and Genomics (ACMG) criteria. Moreover, we identified a heterozygous missense variant in the desmoplakin gene (*DSP*), coding for p.Arg1738Gln, again in the patient and his father. This variant is located in the central α-helical domain (“rod”) of the desmoplakin protein, has an allele frequency of 0.13 in (gnomAD-NFE), and has been classified as benign in ClinVar. Therefore, there is no indication that these sequence variants contribute significantly to the severity of the disease of our patient.

Desmin is absent at intercalated discs in cardiac tissue from the patient

In contrast to normal cardiac tissue with its characteristic desmin labelling of intercalated discs and the extra-sarcomeric cytoskeleton, i.e., the cross-striation pattern (Fig 1E), immunofluorescence microscopy analysis of muscle tissue from the left ventricle of the explanted heart depicted a highly abnormal staining pattern of pathognomonic desmin-positive protein aggregates in conjunction with a lack of desmin at the level of intercalated discs (Figure 1F). To visualize the distribution of the mutant desmin on the subcellular level, we generated a 406W-desmin-specific

rabbit antiserum. In contrast to our standard desmin antiserum (Figure 1E'',F''), which recognizes both wild-type and mutant desmin, the immunoreactivity of the anti-serum to 406W-desmin is restricted to the mutant protein (Figure 1E',F'; Figure 5C). The analysis with both desmin antibodies clearly demonstrated a complete absence of both mutant and wild-type desmin at intercalated discs but a preserved myofibrillar cross-striation signal pattern (Figure 1F,F',F'').

A structural pathology of interacted discs was further corroborated by representative desmoplakin, plectin, N-cadherin, and connexin-43 immunostaining experiments. In contrast to normal control tissue with a co-localization of desmoplakin and desmin at the level of intercalated discs (Figure 2A-A''), our analysis of the diseased heart tissue showed that the desmoplakin signal at intercalated discs was irregular and patchy. Moreover, it was not restricted to intercalated discs but also distributed in a cross-striation type staining pattern throughout the sarcoplasm of cardiomyocytes (Figure 2B-B''). Subsequently, we investigated the effects of the R406W-desmin expression on the subcellular localization of plectin, another member of the plakin family and direct binding partner of desmin. Plectin attaches desmin filaments to strategic anchor sites including myofibrillar Z-discs and cardiac desmosomes [16]. Notably, plectin was no longer detectable at the level of intercalated discs, but kept its characteristic cross-striation signal pattern (Figure 2C-D''). Furthermore, the staining patterns of N-cadherin (Figure 2E-F''), connexin-43 (Figure 2G-H''), and vinculin (data not shown) was irregular and patchy in the patient compared to the distinctly clear restriction to intercalated discs in normal hearts. Since the explanted heart was transferred as a whole into formalin, neither electron microscopic studies nor immunoblots could be performed.

A remarkable mixed pattern with aggregate and filament formation in cultured cells expressing R406W-desmin

To study how mutant desmin in comparison to wild-type desmin would be organized in cells containing an endogenous cytoplasmic intermediate filament network, we transfected mouse 3T3 fibroblasts with R406W-desmin and wild-type desmin, an approach successfully applied for various desmin mutants [17]. Fibroblasts express vimentin, a protein that is co-expressed with and does form copolymers with desmin

in fibroblast-derived myoblasts during all stages of embryonic development [18]. We analyzed the topology of the newly expressed desmin networks 42h after transfection by immunofluorescence microscopy (Figure 3A-D). For the wild-type desmin transfected cells we observed extensive copolymer formation of vimentin (green) and desmin (red), such that parts of the filaments were either stained by both antibodies yielding a merged signal (yellow) or exhibited alternately stained red and green segments indicating that desmin-rich and vimentin-rich unit length filaments (ULFs) and short filament segments of either type did longitudinally anneal (Figure 3A'-A'''). These different types of filaments were even more clear in the cells expressing lower levels of desmin (Figure 3C'-C'''). Again, the mutant desmin did integrate into the vimentin filament system (Figure 3B'-B'''). In some cells, however, a pronounced segregation of vimentin and mutant desmin into short filamentous structures and small protein aggregates as previously observed [17] was evident (Figure 3D,D'-D''').

Subsequently, we investigated the assembly properties of the mutant desmin protein in cells that are devoid of any cytoplasmic intermediate filament protein, i.e., in a spontaneously immortalized cell line derived from embryos of the vimentin knock-out mouse [19]. After transient transfection, R406W-desmin was distributed in numerous dot-like structures throughout the entire cell (data not shown), without any major aggregation foci as observed with several other desmin mutants [20]. Since transient transfection generally leads to high expression of the introduced transgene, we generated in the above vimentin-free fibroblasts cell lines stably expressing R406W-desmin. In parallel, cell lines stably expressing wild-type desmin were generated. For R406W-desmin we isolated 92 stable clones, for wild-type desmin 66 clones. In both cases, three clones with expression of the transgene were selected for further propagation. For wild-type desmin, filamentous arrays extending all over the cell were observed (Figure 3E), whereas for R406W-desmin only small dot-like structures stained positive, with some accumulation around the nucleus as well as at the cell periphery (Figure 3F).

The dual behavior of R406W-desmin *in vitro*: uncoordinated overshoot assembly

For complete and detailed information on the assembly process of desmin intermediate filaments (Figure IA in the Supplement) and the solubility analyses of

mutant and wild-type desmin (Figure IF,G in the Supplement) please refer to the Expanded Results section.

The observation of multiple small aggregates in cardiomyocytes of the reported patient prompted us to have a detailed look at the assembly properties of R406W-desmin to get an idea what kind of structures the subunits of the *in vivo* aggregates could relate to. The first assembly products of the mutant protein, i.e., one to 10 seconds after initiation of assembly in a sodium phosphate-potassium chloride system, were ULFs and short intermediate filaments. Their appearance by electron microscopy was similar to that of wild-type desmin (Figure IB,C in the Supplement), and early growth kinetics of both proteins were in the same range as determined by length measurements of filaments at distinct time points (Figure ID,E in the Supplement). However, already after thirty seconds, R406W-desmin started to form abnormal accumulations of laterally associated filaments making concise filament length determination impossible. This effect was even more pronounced when the assembly conditions were shifted to higher, physiological ionic strength. Whereas wild-type desmin assembled into ULFs and progressively elongating short filaments by ten seconds (Figure 4A), the mutant formed less distinct ULFs than wild-type desmin. In particular, a large number of filaments were of higher diameter and exhibited a more open structure, apparently due to more subunits associating laterally (Figure 4D, arrowheads). In addition, some normal looking filaments were formed, too (Figure 4D, arrows). This hyper-assembly mode continued and accelerated such that within one minute huge, irregularly connected fibre arrays were formed, some parts already depicted sheet-like structures (Figure 4E, arrows) when wild-type desmin formed regular-sized intermediate filaments exclusively (Figure 4B). Furthermore, on occasion individual R406W-desmin filaments were trapped in the process of lateral fusion (Figure 4E, arrowhead). By ten minutes, wild-type desmin exhibited complex intermediate filament networks of single, flexible, and extended filaments (Figure 4C). In stark contrast, R406W-desmin had largely ceased to assemble presenting structures similar to those seen at one minute (Figure 4F).

Remarkably, when R406W-desmin and wild-type desmin were assembled together in equimolar amounts, mixed as monomers before reconstitution from 8 M urea to tetrameric complexes, composite filaments of segments with regular appearance alternating with segments of irregular, wider diameter were formed (Figure 4G).

These *in vitro* assembly data indicate that the mutant protein is fully capable to co-assemble with wild-type desmin and therefore, from a molecular point of view, able to integrate into wild-type desmin filaments. Different from this, filaments became more heterogenous, when ULFs of wild-type desmin and R406W-desmin were mixed after assembling for ten seconds on their own, due to the thicker structures contributed by the mutant protein ULFs (Figure 4H). Nevertheless, this experiment shows that also pure wild-type and R406W-desmin ULFs have a strong capability for longitudinal annealing, and lateral aggregation as seen with the pure mutant protein was not observed as a prominent reaction. For control, wild-type desmin mixed after ten seconds of assembly did assemble normally, excluding that mechanical effects during mixing were influencing the system significantly; on occasion, points of longitudinal annealing were observed (Figure 4I, arrows).

With regard to the aggregates formed by R406W-desmin, we revealed them to be fully soluble in buffers of low ionic strength indicating that, at least *in vitro*, they do not form amyloid-type structures (Figure IF,G in the Supplement). Accordingly, the aggregates present in the tissue sections from the explanted heart did not stain with Congo Red, a staining method for amyloidosis, and therefore indicated the absence of amyloid fibrils (data not shown).

Protein aggregation pathology in striated and smooth muscle tissue of R405W-desmin knock-in mice

We analyzed newly generated R405W-desmin knock-in mice, which harbor the ortholog of the human R406W-desmin. The lower number for the mouse mutation stems from the fact that the murine desmin protein lacks a serine at position 82. Otherwise, the amino acid sequence identity between human and mouse desmin is very high (~98%). For detailed information on the analysis of this mouse model please also refer to the Expanded Results section (Figures II-V in the Supplement). Heterozygous mice were viable and fertile, and showed a normal life span. In contrast, homozygous mice were smaller and already died at the age of 3.4 ± 1.2 month (Figure 5A,B). We analyzed the protein levels of both wild-type desmin and R406W-desmin by immunoblotting in cardiac, skeletal muscle, and smooth muscle tissues using the rabbit antiserum against the carboxy-terminus of desmin (“CT1”)

recognizing both wild-type and mutant desmin protein species as well as the “R406W” rabbit antiserum solely detecting the recombinant human R406W-desmin. Additionally, recombinant proteins were loaded in equal amounts allowing to estimate the relative amounts of wild-type desmin as well as the R405W-desmin in the lysates of the murine muscle tissue specimens (Figure 5C).

Immunofluorescence microscopy demonstrated that both heterozygous and homozygous mice developed a desmin-positive protein aggregate pathology in skeletal muscle tissue with presence of R405W-desmin in small protein aggregates (Figure 5D-F). In analogy to desminopathy patients with heterozygous desmin mutations, analysis of soleus muscles from three-months-old heterozygous desminopathy mice showed a preserved, however, highly irregular cross-striated desmin staining pattern indicating a mis-alignment of myofibrils (Figure 6A,B). In contrast, skeletal muscle from homozygous mice exhibited a marked derangement of the desmin staining pattern with absence of a cross-striation and presence of multiple small subsarcolemmal and sarcoplasmic protein aggregates (Figure 6C). The deleterious effects of R405W-desmin are further highlighted by the analysis of gut smooth muscle tissue from homozygous mice. As seen in skeletal muscle tissue, the normal desmin signal pattern was completely abolished and replaced by a desmin-positive aggregate pathology in both the otherwise intact circular and longitudinal smooth muscle layers from the jejunum (Figure 6D-I). Using an antibody directed against synaptopodin-2, a marker for dense bodies, we could demonstrate an abnormal signal pattern of these structures as well as their co-localization with desmin-positive aggregates (Figure 6J-O). Finally, electron microscopy analysis of duodenal smooth muscle (Figure 6P-S) revealed an abnormal, fuzzy shape of the dense bodies in homozygous mice (Figure 6R,S, arrowheads) compared to wild-type mice (Figure 6P,Q, arrowheads). Moreover, the large granules positive for desmin and synaptopodin-2 in immunofluorescence microscopy are reflected by the presence of 2 to 4 µm large areas apparently consisting of convoluted fibrillar bundles (Figure 6S, asterisk).

Echocardiographic findings of cardiomyopathy in R405W-desminopathy mice

To assess cardiac function, R405W-desminopathy mice were subjected to echocardiography. While young heterozygous animals showed values within the same range as wild-type animals, homozygous mice showed a significantly increased left ventricular ejection fraction as well as a decreased pulmonary acceleration time (PAT) to pulmonary ejection time (PET) ratio (Figure IIIA in the Supplement). In a second experimental group of aged, eighteen-month-old animals, the left ventricular ejection fraction of the heterozygous mice was increased although not reaching statistical significance (Figure IIIA in the Supplement). Moreover, we observed a significantly reduced left ventricular end-diastolic volume and internal diameter and a significantly increased systolic interventricular septum thicknesses indicating development of a distinct cardiomyopathy phenotype in aged mice (Figure IIIA in the Supplement).

Abnormal intercalated discs in R405W-desmin knock-in mice

Immunofluorescence microscopy of hearts from heterozygous R405W-desmin knock-in mice showed desmin in a cross-striated pattern at the level of Z-discs and at the intercalated discs (Figure 7B,E). At higher magnification, the desmin immunofluorescence signal at the Z-discs was found to be uneven with areas displaying a dotted pattern in contrast to the continuous distribution seen in the wild-type tissue specimens (Figure 7A',B',E'). This dotted pattern, prevailed in the cardiac tissue of homozygous animals (Figure 7C',F'). In addition, the distribution of desmoplakin provided evidence of an intercalated disc pathology in heterozygous and more pronounced homozygous mice (Figure 8A-C''). Moreover, at high resolution, desmoplakin staining exhibited widened and fuzzy intercalated discs in the R405W-desmin knock-in mice in conjunction with its partial redistribution to the level of Z-discs (Figure 8B',B'',C',C''), a phenomenon also seen in the analysis of the explanted heart from the heterozygous R406W-desmin patient (Figure 2A-B''). Electron micrographs of ultrathin sections of hearts from wild-type and R405W-desmin knock-in mice (Figure 8D-I) revealed a marked disorganization of the intercalated discs in the desmosomal areas of heterozygous and homozygous animals (Figure 8E,F,H,I, arrowheads). In some regions, a massive disruption of

intercalated discs with multiple lesions, in particular in the homozygous R405W-desmin knock-in mice was evident (Figure 8H,I). In that sense, the fuzzy appearance of intercalated discs seen in immunofluorescence microscopy reflects a robust disturbance of desmosomal junctions sometimes even resulting in a loss of contact between neighboring cardiomyocytes.

Discussion

R406W-desmin: a distinctly cardiotoxic mutant

We have analyzed the pathological consequences for a patient of a *DES* mutation residing in exon 6 and affecting a highly conserved amino acid in the carboxy-terminal end of the α-helical "rod" domain of desmin. The mutation has previously been identified in familial and sporadic patients with desminopathies from various ethnic backgrounds. This particular missense mutation frequently occurs *de novo* making codon 406 to a mutation hot-spot in the human *DES* gene [21-26]. An intriguing feature is its high cardiotoxic potential; in addition to end stage heart failure necessitating heart transplantation, conduction defects, arrhythmias, and sudden cardiac death have been reported in most patients harboring this mutation [26]. Disease onset is typically in an range between 15 to 24 years [22]. In addition to characteristic desmin-positive protein aggregates, our analysis depicted a striking intercalated disc pathology. Besides lack of desmin and plectin at these cell junctions, we observed irregular and patchy N-cadherin and desmoplakin distribution at intercalated discs, a feature that is highly unusual for a cell junction-associated protein. Moreover, desmoplakin was partially re-localized to the level of Z-discs. The findings strongly indicate that expression of the mutant desmin interferes with structural and functional integrity of intercalated discs thereby promoting cardiac pathology. To exclude any effects of additional pathogenic gene variants, we performed targeted next generation sequencing analyses, which identified two more heterozygous variants, i.e., p.Asn761Ser vinculin and p.Arg1738Gln desmoplakin, in the patient as well as in his asymptomatic father. Both variants have been classified as benign polymorphisms.

R406W-desmin exhibits a dual structural and functional state in the basic assembly complexes

For detailed discussion of the structural properties of arginine 406, the *in vitro* assembly of recombinant desmin, and the forced expression of R406W-desmin in cells, please refer to the Expanded Discussion section.

Arginine 406 in desmin is located in the center of an evolutionarily highly conserved 20-amino acid sequence consensus motif at the end of the α-helical rod domain [27]. The amino acid is, together with a similarly conserved motif at the start of α-helical rod domain, instrumental for both the lateral association of tetrameric subunits to ULFs as well as for the subsequent organized end-to-end annealing of ULFs during longitudinal assembly of filaments [28]. Thus, mutations in these segments can impede intermediate filament proteins to assemble beyond the ULF state or may even exacerbate proper ULF formation completely [29].

In contrast to all mutant desmin variants reported thus far, which either integrate into or segregate from the endogenous vimentin intermediate filament system [30], our transfection assays with R406W-desmin in vimentin-containing mouse fibroblasts disclosed a dual pattern of cellular distribution of the mutant protein with formation of small protein aggregates in some cells, whereas other cells displayed normal-appearing desmin intermediate filaments. However, in some often-used intermediate filament-free cell systems such as the human adrenal gland epithelial SW13 line, a segregation may not take place due to the loss of their ability to properly control post-translational assembly of proteins and to mediate a three-dimensional organization of an intermediate filament cytoskeleton. Therefore, co-assembly of a mutant desmin with wild-type desmin may occur in some cases, especially in over-expression situations, to some extent, too [31]. On its own, R406W-desmin did not form extended filament networks in intermediate filament-free cells, but instead assembled into granular structures. This dual pattern can, indeed, be explained from our extensive *in vitro* assembly experiments using recombinant proteins. In particular, the mutant protein does not cause much aggregation when assembled with equimolar amounts of wild-type desmin. Obviously, the wild-type protein is able to rescue the unproductive interactions exhibited by the mutant protein to some extent. Thereby, however, the mutant undercuts the regular filament organization and introduces functionally altered segments into the desmin system. As a consequence, these segments may provide a structurally ambiguous and not mechanical stress-resistant interaction surface for cellular adhesion complexes such as desmosomes and thereby undermine the functional architecture of myocytes.

In summary, the molecular defect in one of desmin's strategic structural domains introduces a functional ambiguity that promotes the development of a malignant

cardiomyopathy.

R405W-desmin knock-in mice: a solid disease model for the human R406W-desminopathy

To study *in vivo* effects of R406W-desmin, we generated and analyzed a R405W-desmin knock-in mouse line, which harbors the ortholog of the human mutation. Heterozygous mice represent a valid genetic animal model for the human disease, because expression of mutant desmin is controlled by endogenous gene regulation sites. Analysis of heterozygous and homozygous mice highlighted the deleterious effect of the R405W-desmin on the structural organization and function of the desmin intermediated filament network in cardiac, skeletal, and smooth muscle tissues. In addition to a protein-aggregate myopathy and cardiomyopathy, homozygous mice developed a smooth muscle-related phenotype with chronic intestinal pseudo-obstruction such that all animals die within the first three month of life. Histopathological analysis of gut smooth muscle disclosed a marked desmin protein aggregation pathology in conjunction with abnormal dense bodies, which act as desmin and actin anchoring sites. In analogy to striated muscle tissue, we conclude that the R405W-desmin-inflicted pathology of the desmin intermediate filament network is the structural basis for the observed reduction in force generation in the small intestine. The importance of this notion is further highlighted by the results obtained for skeletal muscle tissue, which demonstrated clear derangements of the extrasarcomeric desmin cytoskeleton in heterozygous and particularly more pronounced in homozygous mice. These findings agree with and further validate the results from our transfection and *in vitro* assembly experiments with this particular mutant.

Analysis of cardiac tissue from heterozygous and more so from homozygous mice depicted disease-characteristic protein aggregates as well as an intercalated disc pathology comprising aberrant subcellular desmoplakin distribution and desmosomal disintegration. Thus, the mouse model mirrors essential features of the human cardiac pathology highlighting that both murine R405W- and human R406W-desmin interfere with the structural and functional integrity of the cardiac desmin filament network and of intercalated discs. The latter pathology provides an explanation for

conduction defects, arrhythmias, and ventricular contractile dysfunction in R406W-desminopathy patients [22, 24, 26].

Unlike in our patient, we did not detect complete lack of desmin at the level of intercalated discs in heterozygous or homozygous mice. Possibly, the functional organization at the level of intercalated disks differs between man and mice. This assumption seems plausible from a biomechanical point of view as the mouse heart is at least an order of magnitude smaller than the human heart. Moreover, the different life spans of man and mice may also contribute. Therefore, mechanical and age-related aspects will likely differ, including the homeostasis of the multi-component system of intercalated discs, i.e., the *area composita* (for a recent overview see [32]). In this context, genetic background differences may become relevant to some extent, though the fact that all R406W-desmin mutant carriers exhibit an early onset of the disease makes this possibility less likely.

Since R406W-desmin has the potential to form proper unit length filaments, we propose to investigate whether small molecules are able to act as “chemical chaperones” shifting the equilibrium between normally folding and misfolding tetramers to the productive side and may thus help to rescue proper desmin assembly. The observation that 4-phenylbutyrate, a drug approved for the treatment of urea cycle disorders in children [33], ameliorated both desmin aggregation in plectin-deficient mice [34] and mutant keratin aggregation in keratinocytes from patients with epidermolysis bullosa simplex [35] provides a promising prospect.

Conclusion

The cardiotoxic R406W-desmin inflicts its pathogenic potential by a novel pathomechanism with two distinct features, classical formation of protein aggregates containing desmin and generation of an abnormal filament system exhibiting sections of irregular in addition to normal filament morphology. Such chimeric filaments built by mutant and wild-type desmin likely interfere with structural and functional performance of the extra-sarcomeric desmin intermediate filament cytoskeleton. Thus, rather than the presence of pathological protein aggregates as such, the mutant mediates cardiotoxicity presumably by compromising attachment of “hybrid” desmin filaments to desmosomes, thereby destabilizing intercalated discs. Detection

of a heterozygous *DES* mutation leading to p.R406W-desmin may trigger a careful electrophysiological assessment including discussion of the early implantation of a pacemaker/cardioverter defibrillator device to prevent sudden cardiac death. State-of-the-art molecular risk stratification of individual desmin mutations should encompass a multi-disciplinary experimental approach comprising assessment of the tissue pathology in conjunction with genome analysis and *in vitro* desmin assembly studies. However, for the *in vivo* validation of individual desmin mutations, patient-mimicking cell and animal models are still indispensable.

Acknowledgements

The authors thank the following persons and institutions: Onnik Agbulut, ABV, UMR 8256, Paris, France, for discussion regarding striated muscles. Sabria Allithi, Jacques Monod Institutes, Paris, France, for genotyping of mice. Jennifer Alonso, the Animalliance company, Paris, France, for carefully handling animals. Delphine Delacour, Cell Adhesion and Mechanics, IJM, Paris, France, for suggestions and discussions on the intestinal tract. Florence Delort, BFA, UMR 8251, Paris, France, for advices on skeletal muscle treatment. Frédéric Fiore, Centre for Immunophenomics, Marseille, France, for generating the R405W desmin knock-in mice. Michaela Hergt, Molecular Genetics, B060, German Cancer Research Center, Heidelberg, Germany, for her help in the pre-phase of transfection experiments. HISTIM histology platform, Cochin institute, Paris, France, for tissue sections. Andreas Hofmann, Griffith University, Nathan, Australia, for *in silico* analysis and discussion regarding the desmoplakin variant. Elena Honscheid, Institute of Aerospace Medicine, German Aerospace Center, Cologne, Germany, for video processing. Jens Jordan, Institute of Aerospace Medicine, German Aerospace Center, Cologne, Germany, for discussion of the manuscript. Lisa Kamm, Institute of Neuropathology, University Hospital Erlangen, Erlangen, Germany, for immunoblot and immunofluorescence experiments as well as cell culture work. Frank Lager, Cochin Institute, Paris, France, for echography investigations. Zhenlin Li, ABV, UMR 8256, Paris, France, for discussion regarding desmin knock-in and knock-out mice. Nicole Mack, Institute of Neuropathology, University Hospital Erlangen, Erlangen, Germany, for the redrawing of the desmin filament assembly schematic. Carmen Marchiol, Cochin Institute, Paris, France, for echography investigations. Norbert Mücke, Chromatin Networks, B066, German Cancer Research Center, Heidelberg, Germany, for generating assembly statistics. Isabelle Le Parco, head of the Buffon animal facility, Paris, France, for judicious advices about mice management. Denise Paulin, ABV, UMR 8256, Paris, France, for discussion regarding the intestinal phenotype. Camélia Piat, the Animalliance company, Paris, France, for managing the mouse colony. Sabrina Pichon, BFA, UMR 8251, Paris, France, for advices on skeletal muscle treatment. Gilles Renault, Cochin Institute, Paris, France, for analyses at the "Platform for small animals". Karsten Richter, Imaging and Cytometry Core Facility, Electron Microscopy, W230, German Cancer Research Center, Heidelberg, Germany, for providing electron microscopic images. Sergei V. Strelkov,

Katholieke Universiteit Leuven, Leuven, Belgium, for discussion regarding the desmoplakin variant. Tatjana Wedig, Pediatric Neurooncology, B062, German Cancer Research Center, Heidelberg, Germany, for generating recombinant desmin, performing assembly experiments, and electron microscopy.

Sources of Funding

This work was supported by the German Research Foundation (DFG), grants HE 1853/4-3 and HE 1853/11-1 to HH and SCHR 562/15-1 to RS, by the Fondation maladies rares, grant MOM201311 to AL, by the Association Française contre les Myopathies (AFM), grant 20802 to AL, and by the Agence Nationale de la Recherche (ANR), grant ANR-13-BSV5-0017 to AL. EC and PV were supported by Paris Diderot University, NC and AL by the French National Centre for Scientific Research (CNRS), and AF by the National Institute for Medical Research (INSERM). MS was supported by the Interdisciplinary Center for Clinical Research (IZKF) of the Clinical Center Erlangen. BM was supported by an excellence fellowship of the Else Kröner-Fresenius Foundation. BM, OJM, and HAK were supported by the German Center for Cardiovascular Research (DZHK). Part of this work was also supported by grants from the Informatics for Life (Klaus Tschira Foundation), and the European Union (DETECTIN-HF).

Disclosures

The authors have no conflict of interest to declare.

Supplemental Materials

Expanded Materials and Methods
Expanded Results
Expanded Discussion
Supplemental Figures I - V
Supplemental Movie I
References 36 - 57

References

1. Clemen CS, Herrmann H, Strelkov SV, Schröder R. Desminopathies: pathology and mechanisms. *Acta Neuropathol*. 2013;125:47-75.
2. Hnia K, Ramspacher C, Vermot J, Laporte J. Desmin in muscle and associated diseases: beyond the structural function. *Cell Tissue Res*. 2015;360:591-608.
3. Brodehl A, Gaertner-Rommel A, Milting H. Molecular insights into cardiomyopathies associated with desmin (DES) mutations. *Biophysical reviews*. 2018;10:983-1006.
4. Capetanaki Y, Papathanasiou S, Diokmetzidou A, Vatsellas G, Tsikitis M. Desmin related disease: a matter of cell survival failure. *Curr Opin Cell Biol*. 2015;32:113-120.
5. van Spaendonck-Zwarts K, van Hessem L, Jongbloed JD, de Walle HE, Capetanaki Y, van der Kooi AJ, van Langen IM, van den Berg MP, van Tintelen JP. Desmin-related myopathy: a review and meta-analysis. *Clin Genet*. 2010;80:354-366.
6. Carmignac V, Sharma S, Arbogast S, Fischer D, Serreri C, Serria M, Stoltenburg G, Maurage CA, Herrmann H, Cuisset JM, et al. A homozygous desmin deletion causes an Emery-Dreifuss like recessive myopathy with desmin depletion. *Neuromuscul Disord*. 2009;19:600.
7. Durmus H, Ayhan O, Cirak S, Deymeer F, Parman Y, Franke A, Eiber N, Chevessier F, Schlotzer-Schrehardt U, Clemen CS, et al. Neuromuscular endplate pathology in recessive desminopathies: Lessons from man and mice. *Neurology*. 2016;87:799-805.
8. Henderson M, De Waele L, Hudson J, Eagle M, Sewry C, Marsh J, Charlton R, He L, Blakely EL, Horrocks I, et al. Recessive desmin-null muscular dystrophy with central nuclei and mitochondrial abnormalities. *Acta Neuropathol*. 2013;125:917-919.
9. McLaughlin HM, Kelly MA, Hawley PP, Darras BT, Funke B, Picker J. Compound heterozygosity of predicted loss-of-function DES variants in a family with recessive desminopathy. *BMC Med Genet*. 2013;14:68.
10. Riley LG, Waddell LB, Ghaoui R, Evesson FJ, Cummings BB, Bryen SJ, Joshi H, Wang MX, Brammah S, Kritharides L, et al. Recessive DES cardio/myopathy without myofibrillar aggregates: intronic splice variant silences one allele leaving only missense L190P-desmin. *Eur J Hum Genet*. 2019;27:1267-1273.
11. Arbustini E, Morbini P, Grasso M, Fasani R, Verga L, Bellini O, Dal Bello B, Campana C, Piccolo G, Febo O, et al. Restrictive cardiomyopathy, atrioventricular block and mild to subclinical myopathy in patients with desmin-immunoreactive material deposits. *J Am Coll Cardiol*. 1998;31:645-653.
12. Cetin N, Balci-Hayta B, Gundesli H, Korkusuz P, Purali N, Talim B, Tan E, Selcen D, Erdem-Ozdamar S, Dincer P. A novel desmin mutation leading to autosomal recessive limb-girdle muscular dystrophy: distinct histopathological outcomes compared with desminopathies. *J Med Genet*. 2013;50:437-443.
13. Goldfarb LG, Park KY, Cervenakova L, Gorokhova S, Lee HS, Vasconcelos O, Nagle JW, Semino-Mora C, Sivakumar K, Dalakas MC. Missense mutations in desmin associated with familial cardiac and skeletal myopathy. *Nat Genet*. 1998;19:402-403.
14. Munoz-Marmol AM, Strasser G, Isamat M, Coulombe PA, Yang Y, Roca X, Vela E, Mate JL, Coll J, Fernandez-Figueras MT, et al. A dysfunctional desmin mutation in a patient with severe generalized myopathy. *Proc Natl Acad Sci USA*. 1998;95:11312-11317.
15. Pinol-Ripoll G, Shatunov A, Cabello A, Larrode P, de la Puerta I, Pelegrin J, Ramos FJ, Olive M, Goldfarb LG. Severe infantile-onset cardiomyopathy associated with a homozygous deletion in desmin. *Neuromuscul Disord*. 2009;19:418-422.
16. Konieczny P, Fuchs P, Reipert S, Kunz WS, Zeöld A, Fischer I, Paulin D, Schröder R, Wiche G. Myofiber integrity depends on desmin network targeting to Z-disks and costameres via distinct plectin isoforms. *J Cell Biol*. 2008;181:667-681.
17. Bär H, Kostareva A, Sjoberg G, Sejersen T, Katus HA, Herrmann H. Forced expression of desmin and desmin mutants in cultured cells: impact of myopathic missense mutations in the central coiled-coil domain on network formation. *Exp Cell Res*. 2006;312:1554-1565.
18. Lazarides E. Intermediate filaments: a chemically heterogeneous, developmentally regulated class of proteins. *Annu Rev Biochem*. 1982;51:219-250.
19. Colucci-Guyon E, Portier MM, Dunia I, Paulin D, Pournin S, Babinet C. Mice lacking

vimentin develop and reproduce without an obvious phenotype. *Cell*. 1994;79:679-694.
20. Bär H, Mücke N, Ringler P, Müller SA, Kreplak L, Katus HA, Aebi U, Herrmann H. Impact of disease mutations on the desmin filament assembly process. *J Mol Biol*. 2006;360:1031-1042.
21. Arbustini E, Pasotti M, Pilotto A, Pellegrini C, Grasso M, Previtali S, Repetto A, Bellini O, Azan G, Scaffino M, et al. Desmin accumulation restrictive cardiomyopathy and atrioventricular block associated with desmin gene defects. *Eur J Heart Fail*. 2006;8:477-483.
22. Dagvadorj A, Olive M, Urtizberea JA, Halle M, Shatunov A, Bonnemann C, Park KY, Goebel HH, Ferrer I, Vicart P, et al. A series of West European patients with severe cardiac and skeletal myopathy associated with a de novo R406W mutation in desmin. *J Neurol*. 2004;251:143-149.
23. Dalakas MC, Park KY, Semino-Mora C, Lee HS, Sivakumar K, Goldfarb LG. Desmin myopathy, a skeletal myopathy with cardiomyopathy caused by mutations in the desmin gene. *N Engl J Med*. 2000;342:770-780.
24. Olive M, Goldfarb L, Moreno D, Laforet E, Dagvadorj A, Sambuughin N, Martinez-Matos JA, Martinez F, Alio J, Farrero E, et al. Desmin-related myopathy: clinical, electrophysiological, radiological, neuropathological and genetic studies. *J Neurol Sci*. 2004;219:125-137.
25. Park KY, Dalakas MC, Semino-Mora C, Lee HS, Litvak S, Takeda K, Ferrans VJ, Goldfarb LG. Sporadic cardiac and skeletal myopathy caused by a de novo desmin mutation. *Clin Genet*. 2000;57:423-429.
26. Wahbi K, Behin A, Charron P, Dunand M, Richard P, Meune C, Vicart P, Laforet P, Stojkovic T, Becane HM, et al. High cardiovascular morbidity and mortality in myofibrillar myopathies due to DES gene mutations: a 10-year longitudinal study. *Neuromuscul Disord*. 2012;22:211-218.
27. Herrmann H, Strelkov SV, Feja B, Rogers KR, Brettel M, Lustig A, Häner M, Parry DA, Steinert PM, Burkhard P, et al. The intermediate filament protein consensus motif of helix 2B: its atomic structure and contribution to assembly. *J Mol Biol*. 2000;298:817-832.
28. Herrmann H, Strelkov SV, Burkhard P, Aebi U. Intermediate filaments: primary determinants of cell architecture and plasticity. *J Clin Invest*. 2009;119:1772-1783.
29. Premchandar A, Mücke N, Poznanski J, Wedig T, Kaus-Drobek M, Herrmann H, Dadlez M. Structural Dynamics of the Vimentin Coiled-coil Contact Regions Involved in Filament Assembly as Revealed by Hydrogen-Deuterium Exchange. *J Biol Chem*. 2016;291:24931-24950.
30. Bär H, Mücke N, Kostareva A, Sjoberg G, Aebi U, Herrmann H. Severe muscle disease-causing desmin mutations interfere with in vitro filament assembly at distinct stages. *Proc Natl Acad Sci USA*. 2005;102:15099-15104.
31. Brodehl A, Hedde PN, Dieding M, Fatima A, Walhorn V, Gayda S, Saric T, Klauke B, Gummert J, Anselmetti D, et al. Dual color photoactivation localization microscopy of cardiomyopathy-associated desmin mutants. *J Biol Chem*. 2012;287:16047-16057.
32. Green KJ, Jaiganesh A, Broussard JA. Desmosomes: Essential contributors to an integrated intercellular junction network. *F1000Research*. 2019;8:F1000 Faculty Rev-2150.
33. Guha M. Urea cycle disorder drug approved. *Nat Biotechnol*. 2013;31:274.
34. Winter L, Staszewska I, Mihailovska E, Fischer I, Goldmann WH, Schröder R, Wiche G. Chemical chaperone ameliorates pathological protein aggregation in plectin-deficient muscle. *J Clin Invest*. 2014;124:1144-1157.
35. Spörrer M, Prochnicki A, Tolle RC, Nystrom A, Esser PR, Homberg M, Athanasiou I, Zingkou E, Schilling A, Gerum R, et al. Treatment of keratinocytes with 4-phenylbutyrate in epidermolysis bullosa: Lessons for therapies in keratin disorders. *EBioMedicine*. 2019;44:502-515.
36. Desgrange A, Lokmer J, Marchiol C, Houyel L, Meilhac SM. Standardised imaging pipeline for phenotyping mouse laterality defects and associated heart malformations, at multiple scales and multiple stages. *Dis Model Mech*. 2019;12:dmm038356.

37. Gregor M, Osmanagic-Myers S, Burgstaller G, Wolfram M, Fischer I, Walko G, Resch GP, Jorgl A, Herrmann H, Wiche G. Mechanosensing through focal adhesion-anchored intermediate filaments. *FASEB J*. 2014;28:715-729.
38. Meier M, Padilla GP, Herrmann H, Wedig T, Hergt M, Patel TR, Stetefeld J, Aebi U, Burkhard P. Vimentin coil 1A-A molecular switch involved in the initiation of filament elongation. *J Mol Biol*. 2009;390:245-261.
39. Gunning P, Leavitt J, Muscat G, Ng SY, Kedes L. A human beta-actin expression vector system directs high-level accumulation of antisense transcripts. *Proc Natl Acad Sci USA*. 1987;84:4831-4835.
40. Niehrs C, Huttner WB, Ruther U. In vivo expression and stoichiometric sulfation of the artificial protein sulfophilin, a polymer of tyrosine sulfation sites. *J Biol Chem*. 1992;267:15938-15942.
41. Schröder R, Warlo I, Herrmann H, van der Ven PF, Klasen C, Blümcke I, Mundegar RR, Fürst DO, Goebel HH, Magin TM. Immunogold EM reveals a close association of plectin and the desmin cytoskeleton in human skeletal muscle. *Eur J Cell Biol*. 1999;78:288-295.
42. Koeser J, Troyanovsky SM, Grund C, Franke WW. De novo formation of desmosomes in cultured cells upon transfection of genes encoding specific desmosomal components. *Exp Cell Res*. 2003;285:114-130.
43. Herrmann H, Kreplak L, Aebi U. Isolation, characterization, and in vitro assembly of intermediate filaments. *Methods Cell Biol*. 2004;78:3-24.
44. Chopard A, Pons F, Charpiot P, Marini JF. Quantitative analysis of relative protein contents by Western blotting: comparison of three members of the dystrophin-glycoprotein complex in slow and fast rat skeletal muscle. *Electrophoresis*. 2000;21:517-522.
45. Clemen CS, Stöckigt F, Strucksberg KH, Chevessier F, Winter L, Schütz J, Bauer R, Thorweihe JM, Wenzel D, Schlötzer-Schrehardt U, et al. The toxic effect of R350P mutant desmin in striated muscle of man and mouse. *Acta Neuropathol*. 2015;129:297-315.
46. Herrmann H, Häner M, Brettel M, Ku NO, Aebi U. Characterization of distinct early assembly units of different intermediate filament proteins. *J Mol Biol*. 1999;286:1403-1420.
47. Mücke N, Kammerer L, Winheim S, Kirmse R, Krieger J, Mildenberger M, Bassler J, Hurt E, Goldmann WH, Aebi U, et al. Assembly Kinetics of Vimentin Tetramers to Unit-Length Filaments: A Stopped-Flow Study. *Biophys J*. 2018;114:2408-2418.
48. Wickert U, Mücke N, Wedig T, Müller SA, Aebi U, Herrmann H. Characterization of the in vitro co-assembly process of the intermediate filament proteins vimentin and desmin: mixed polymers at all stages of assembly. *Eur J Cell Biol*. 2005;84:379-391.
49. Bär H, Schopferer M, Sharma S, Hochstein B, Mücke N, Herrmann H, Willenbacher N. Mutations in Desmin's Carboxy-Terminal "Tail" Domain Severely Modify Filament and Network Mechanics. *J Mol Biol*. 2010;397:1188-1198.
50. Kirmse R, Portet S, Mücke N, Aebi U, Herrmann H, Langowski J. A quantitative kinetic model for the in vitro assembly of intermediate filaments from tetrameric vimentin. *J Biol Chem*. 2007;282:18563-18572.
51. Ramm B, Stigler J, Hinczewski M, Thirumalai D, Herrmann H, Woehlke G, Rief M. Sequence-resolved free energy profiles of stress-bearing vimentin intermediate filaments. *Proc Natl Acad Sci USA*. 2014;111:11359-11364.
52. Schaffeld M, Herrmann H, Schultess J, Markl J. Vimentin and desmin of a cartilaginous fish, the shark Scyliorhinus stellaris: sequence, expression patterns and in vitro assembly. *Eur J Cell Biol*. 2001;80:692-702.
53. Kapinos LE, Schumacher J, Mücke N, Machaidze G, Burkhard P, Aebi U, Strelkov SV, Herrmann H. Characterization of the head-to-tail overlap complexes formed by human lamin A, B1 and B2 "half-minilamin" dimers. *J Mol Biol*. 2010;396:719-731.
54. Rainer PP, Dong P, Sorge M, Fert-Bober J, Holewinski RJ, Wang Y, Foss CA, An SS, Baracca A, Solaini G, et al. Desmin Phosphorylation Triggers Preamyloid Oligomers Formation and Myocyte Dysfunction in Acquired Heart Failure. *Circ Res*. 2018;122:e75-e83.

55. Quinlan RA, Franke WW. Heteropolymer filaments of vimentin and desmin in vascular smooth muscle tissue and cultured baby hamster kidney cells demonstrated by chemical crosslinking. *Proc Natl Acad Sci USA*. 1982;79:3452-3456.
56. Rogers KR, Herrmann H, Franke WW. Characterization of disulfide crosslink formation of human vimentin at the dimer, tetramer, and intermediate filament levels. *J Struct Biol*. 1996;117:55-69.
57. Kolb T, Maass K, Hergt M, Aebi U, Herrmann H. Lamin A and lamin C form homodimers and coexist in higher complex forms both in the nucleoplasmic fraction and in the lamina of cultured human cells. *Nucleus*. 2011;2:425-433.

Figure Legends

Figure 1

R406W-desmin-related human cardiac pathology. (**A**,**B**) Cardiac magnetic resonance imaging illustrating large right and left atria as a sign of increasing restrictive cardiomyopathy in a four-chamber view (**A**) and diffuse transmyocardial late gadolinium-enhancement (**B**) in the wall of the left ventricle (arrowhead). (**C**,**D**) Sirius red stains of normal control and the diseased cardiac tissue. Note the massive interstitial fibrosis in the R406W-desmin heart (**D**). For the purpose of this study, we generated a polyclonal rabbit antiserum specifically recognizing the mutant, R406W-desmin, but not the wild-type protein (**E‘,F‘**). In normal heart tissue desmin immunolabeling is present at the level of intercalated discs and at the interspace between neighboring myofibrillar Z-discs thus giving rise to the typical cross-striated staining pattern of cardiomyocytes (**E**,**E‘‘**); arrowheads, autofluorescence signal of lipofuscin. Note the markedly altered desmin staining pattern in the diseased heart with the presence of protein aggregates and a lack of intercalated disc labelling (**F**). However, at higher magnification, R406W-desmin still displayed a preserved myofibrillar cross-striation signal pattern (**F‘**,**F‘‘**).

Figure 2

Desmoplakin, plectin, N-cadherin, connexin-43, and desmin immunostains of cardiac tissue specimens from patient and normal control. Double immunostaining of desmoplakin and desmin (**A**,**B**), plectin and desmin (**C**,**D**), N-cadherin and desmin (**E**,**F**) as well as connexin-43 and desmin (**G**,**H**) in normal (**A**,**C**,**E**,**G**) and diseased (**B**,**D**,**F**,**H**) heart tissue. Note the co-localization (yellow) of desmoplakin and desmin at the level of intercalated discs in normal cardiac tissue (**A**,**A‘**,**A‘‘**), whereas the analysis of the tissue from the patient depicted irregular and patchy stains of both proteins at these structures (**B**,**B‘**,**B‘‘**). Notably, the desmoplakin signal was no longer restricted to the intercalated discs, but also visible at the level of Z-discs (**B‘‘**). The presence of R406W-desmin also leads to an altered subcellular distribution of plectin, which is no longer present at the level of intercalated discs (**C**,**D**). Note that the desmin-positive protein aggregates (**D‘**, asterisk) are devoid of

plectin staining (**D‘‘**). The intercalated disc pathology is further highlighted by N-cadherin stains (**E**,**F**); note that the co-localization of desmin and N-cadherin, which was observed in normal tissue (**E‘**,**E‘‘**), was abrogated and that the N-cadherin signal also became irregular and patchy in the patient (**E‘‘**,**F‘‘**). The desmin pathology in the explanted heart (**H**,**H‘**) did also result in an obviously changed connexin-43 signal pattern (**G‘‘**,**H‘‘**). Pictures (A) and (E) as well as (B) and (F) are from the same triple-fluorescence images.

Figure 3

Transfection of desmin into fibroblasts. (**A**-**D**) Murine 3T3 fibroblasts were transiently transfected with human wild-type desmin (**A**,**C**) and R406W-desmin (**B**,**D**) and stained with vimentin-specific (green) and desmin-specific (red) antibodies. Higher magnified areas depict copolymer formation of desmin and vimentin (**A‘**-**C‘‘‘**) and segregation R406W-desmin and vimentin (**D‘**-**D‘‘‘**). (**E**,**F**) Representative cells from stable clones expressing human wild-type desmin (**E**) and R406W-desmin (**F**) in mouse vimentin knock-out ($Vim^{-/-}$) fibroblasts were stained with antibodies specific for desmin.

Figure 4

Electron micrographs of *in vitro* assembly structures generated by wild-type desmin and R406W-desmin. Wild-type desmin (**A**-**C**) and R406W-desmin (**D**-**F**) were assembled in 25 mM Tris-HCl, pH 7.5, 160 mM sodium chloride; assembly was stopped by fixation after 10 s (**A**,**D**), 1 min (**B**,**E**) and 10 min (**C**,**F**). In (**D**), arrows indicate single ULFs, arrowheads point to large diameter ULFs and filament segments. In (**E**), arrows indicate sheet-like structures, the arrowhead highlights a filament in the process of lateral fusion. (**G**-**I**) Co-assembly experiments of R406W-desmin and wild-type desmin under different conditions. (**G**) R406W-desmin and wild-type desmin were mixed as monomers in urea in a 1:1 ratio before being renatured to tetramers and assembled for 10 min. Arrowheads indicate normal diameter filament segments; arrows point to unusually thick, compacted filaments; white arrows highlight lateral fusion events. (**H**) Both proteins were assembled

separately for 10 s – at what time point they form ULFs and short intermediate filaments – and were then mixed and incubated for another 10 min. Arrows, thick filament segments obviously originating from R406W-desmin; arrowheads, segments of normal diameter probably originating from wild-type desmin. Note that ends of normal diameter intermediate filaments can longitudinally anneal with the ends of thick filaments. (**I**) Aliquots of wild-type desmin were preassembled separately for 10 s, mixed and were then assembled for 10 min to control for potential mechanical disturbances during the mixing process. Arrows indicate annealing sites of individual filament segments.

Figure 5

Analysis of newly generated R405W-desmin knock-in mice. (**A**) Representative photographs of wild-type (wt), heterozygous (het), and homozygous (hom) siblings at the age of three months. Homozygous mice have a significantly smaller body size and reduced body weight (Figure IIC,D in the Supplement). (**B**) Survival curve of mice of all three genotypes. Homozygous mice die prematurely at a mean age of 3.4 ± 1.2 months (dashed line). (**C**) Desmin immunoblotting of cardiac, skeletal, and smooth muscle tissue lysates from the R405W desminopathy mice. For this purpose, two newly generated rabbit polyclonal antibody were used. While the “CT1” antiserum recognizes both wild-type and mutant desmin protein species (total desmin), the “DesR406W” antiserum solely recognizes human R406W-desmin and the orthologous murine R405W-desmin (R405/6W desmin). Samples of recombinant, purified human wild-type and R406W-desmin were loaded as positive controls. Equal loading of the murine tissue samples from wild-type and heterozygous R405W-desmin knock-in mice is demonstrated by the Coomassie Brilliant Blue stained SDS-PAGE gels. (**D**-**F**) Presence of R405W-desmin in small protein aggregates in transverse sections of soleus muscle from heterozygous and homozygous mice detected by the mutant-specific antiserum. Asterisks, low-intensity autofluorescence in the subsarcolemmal region of the wild-type soleus specimen. Images were deconvolved using Huygens Essential (Scientific Volume Imaging).

Figure 6

Effects of R405W-desmin on skeletal and smooth muscle tissue. (**A**-**C**) Longitudinal sections of soleus muscles stained for desmin (wild-type and mutant) and nuclei (DAPI). While wild-type muscle displayed a regular cross-striation pattern (**A'**), the desmin staining in heterozygous and homozygous muscles was highly abnormal. Note the irregular and absent cross-striation in heterozygous and homozygous mice, respectively (**B'**,**C'**), as well as the accumulation of mutant desmin in the subsarcolemmal region of soleus muscle fibers from homozygous mice (arrowheads). (**D**-**I**) The noxious effect of R405W-desmin was further highlighted in the comparative analysis of longitudinal sections of the jejunal muscularis propria from wild-type and homozygous mice. In contrast to the desmin and smooth muscle actin staining patterns in the wild-type, homozygous mice displayed the absence of a desmin intermediate filament cytoskeleton and instead the presence of a marked desmin protein aggregation pathology. lm, longitudinal muscle layer; cm, circular muscle layer. (**J**-**O**) Further analysis using an antibody directed against synaptopodin-2, an established marker for dense bodies, showed a partial co-localization with R405W-desmin-positive aggregates in smooth muscle of the duodenum (arrowheads). (**P**-**S**) Ultrastructural analysis of duodenal smooth muscle tissue from wild-type and homozygous mice. Note the presence of abnormally shaped dense bodies (arrowheads) as well as the presence of large areas of electron-dense material representing protein aggregates (asterisk).

Figure 7

Desmin immunostains of cardiac tissue specimens from R405W-desminopathy mice. Immunofluorescence microscopic analysis of cardiac tissue specimens from wild-type (**A**,**D**), heterozygous (**B**,**E**), and homozygous (**C**,**F**) R405W-desmin knock-in mice. In contrast to the findings in the human R406W-desmin heart, intercalated discs in the murine desminopathy cardiac tissue display a labelling with both the antibody recognizing wild-type and R405W mutant desmin (total desmin) and the antibody specifically directed against the point mutated desmin protein species (arrowheads). As seen in the human R406W-desmin heart, the mutant desmin retains its ability to localize to the level of myofibrillar Z-bands resulting in the typical

cross-striated staining pattern. Images were deconvolved using Huygens Essential (Scientific Volume Imaging).

Figure 8

Desmoplakin and desmin double-immunostains and transmission electron microscopy of cardiac tissue specimens from R405W-desminopathy mice. Immunofluorescence microscopic analysis of cardiac tissue specimens from wild-type (**A**), heterozygous (**B**), and homozygous (**C**) R405W-desmin knock-in mice. Note the irregular desmoplakin signal at the level of intercalated discs and the partial sarcoplasmic redistribution of desmoplakin to the level of Z-discs co-localizing with the desmin signal. Images were deconvolved using Huygens Essential (Scientific Volume Imaging). (**D**-**I**) Ultrastructural analysis of intercalated discs revealed a marked derangement of the electron-dense desmosomal regions (arrowheads) in heterozygous (**E**,**H**) and homozygous (**F**,**I**) mice as compared to the wild-type (**D**,**G**). Asterisks, areas containing polyform membranous structures. Hashtag, ruptures of the intercalated disc between two cardiomyocytes were occasionally observed. M, mitochondria; Z, Z-bands.

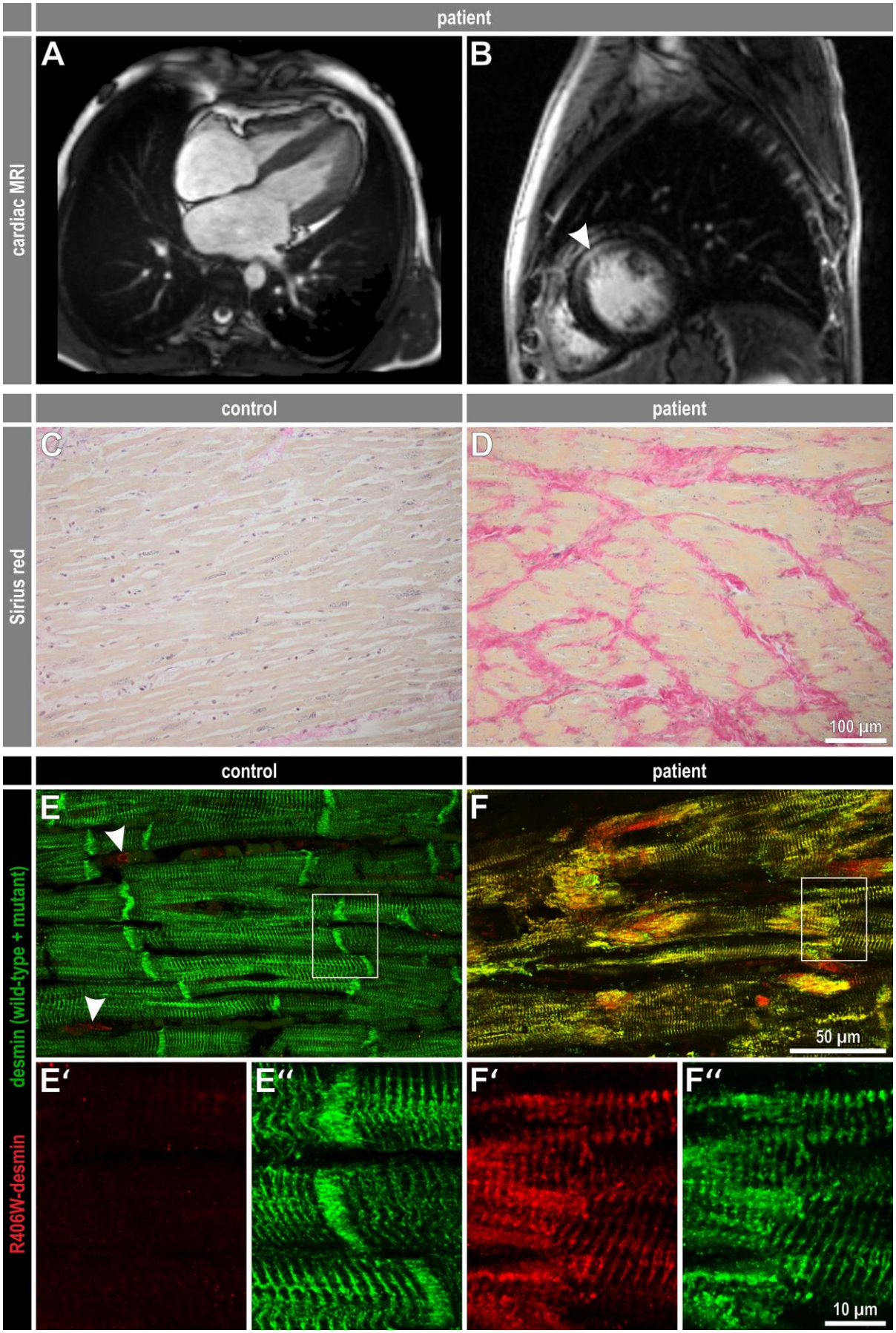
patient
cardiac MRI
A
B
control
patient
Sirius red
C
D
100 µm
control
patient
desmin (wild-type + mutant)
R406W-desmin
E
F
50 µm
E'
E''
F'
F''
10 µm

Figure 1

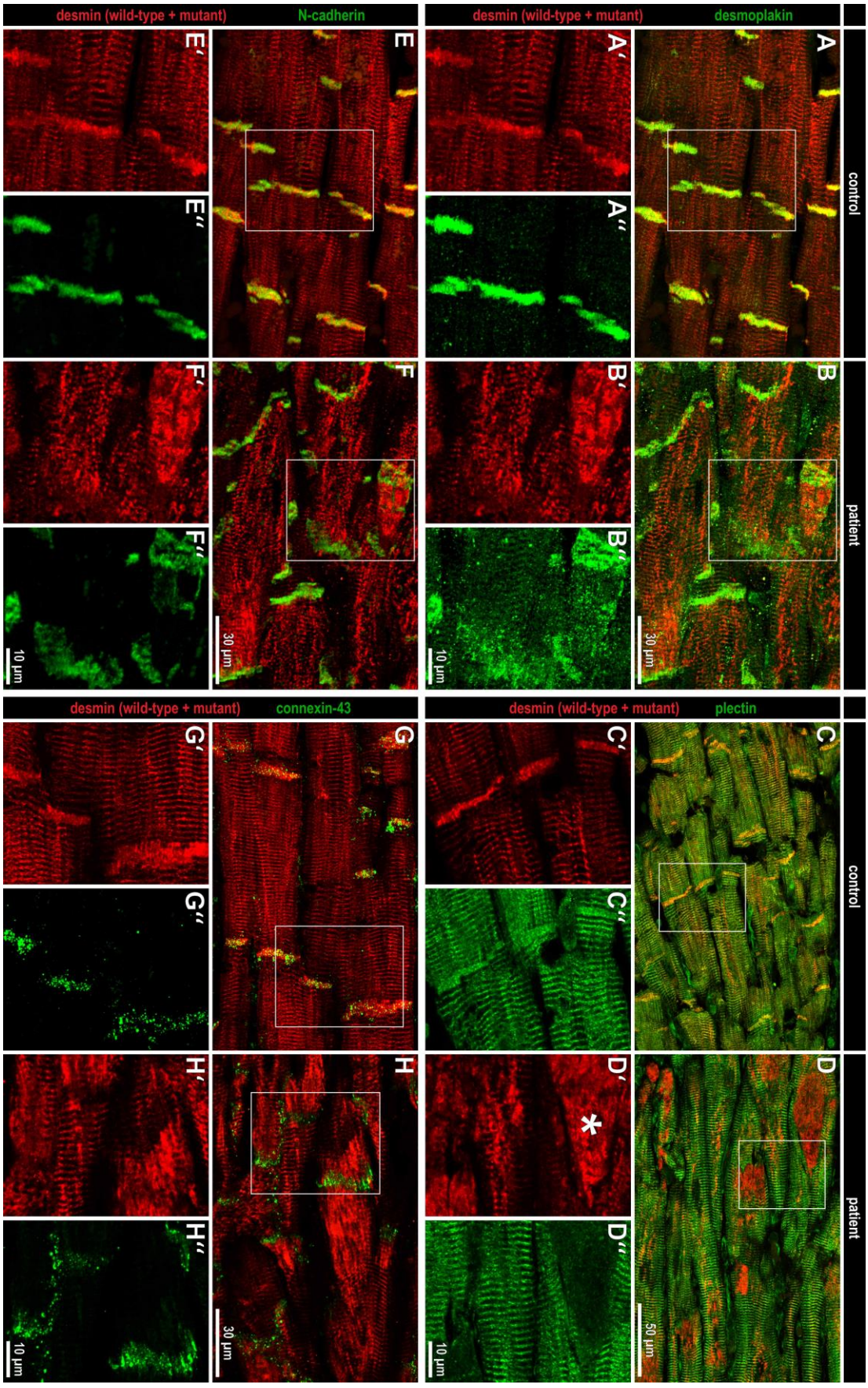
control
patient
desmoplakin
desmin (wild-type + mutant)
plectin
N-cadherin
connexin-43
A
A′
A″
B
B′
B″
C
C′
C″
D
D′
D″
E
E′
E″
F
F′
F″
G
G′
G″
H
H′
H″
50 µm
30 µm
10 µm
*

Figure 2

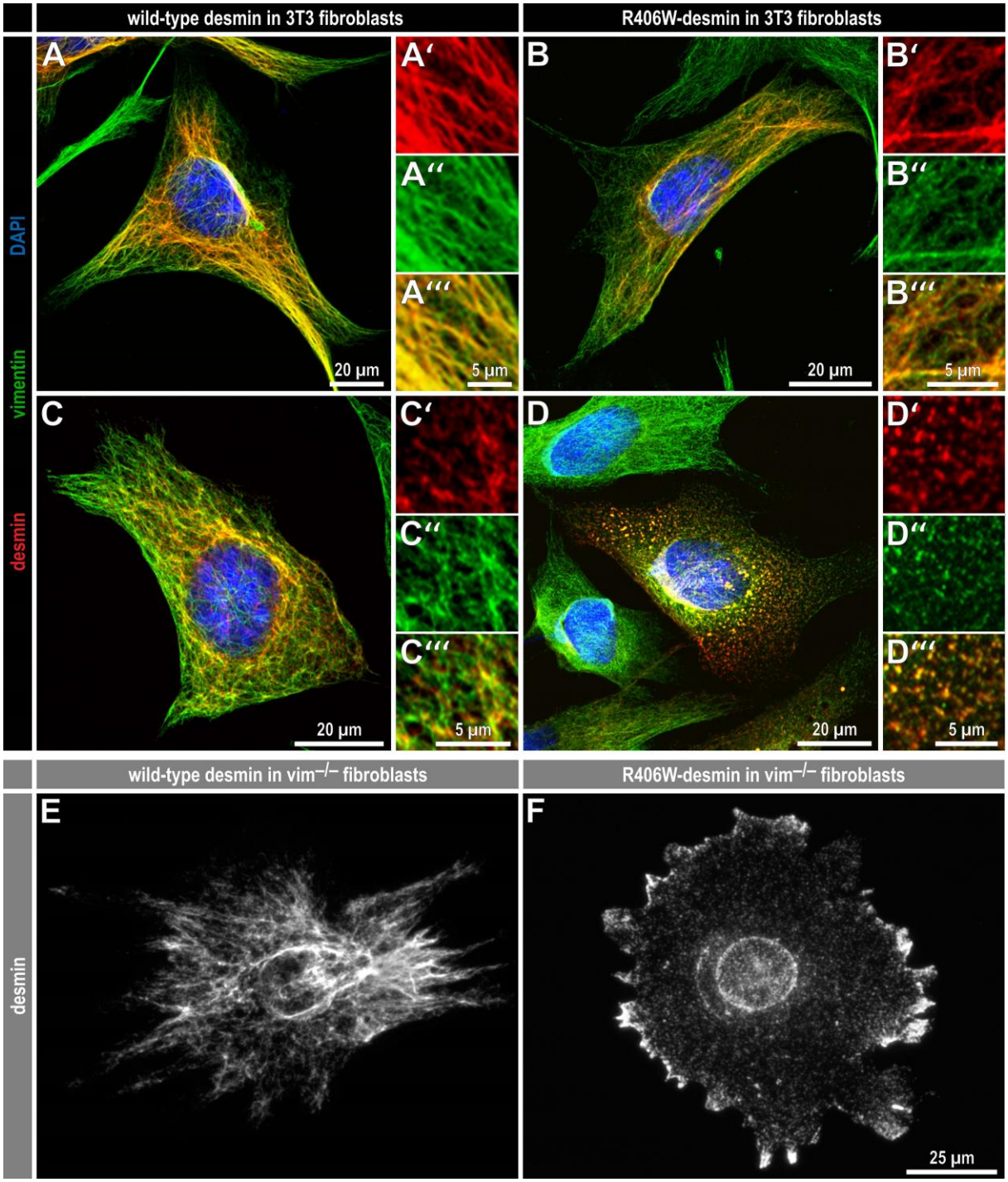
wild-type desmin in 3T3 fibroblasts
R406W-desmin in 3T3 fibroblasts
DAPI
vimentin
desmin
A
A'
A''
A'''
B
B'
B''
B'''
C
C'
C''
C'''
D
D'
D''
D'''
20 µm
5 µm
wild-type desmin in vim−/− fibroblasts
R406W-desmin in vim−/− fibroblasts
E
F
25 µm

Figure 3

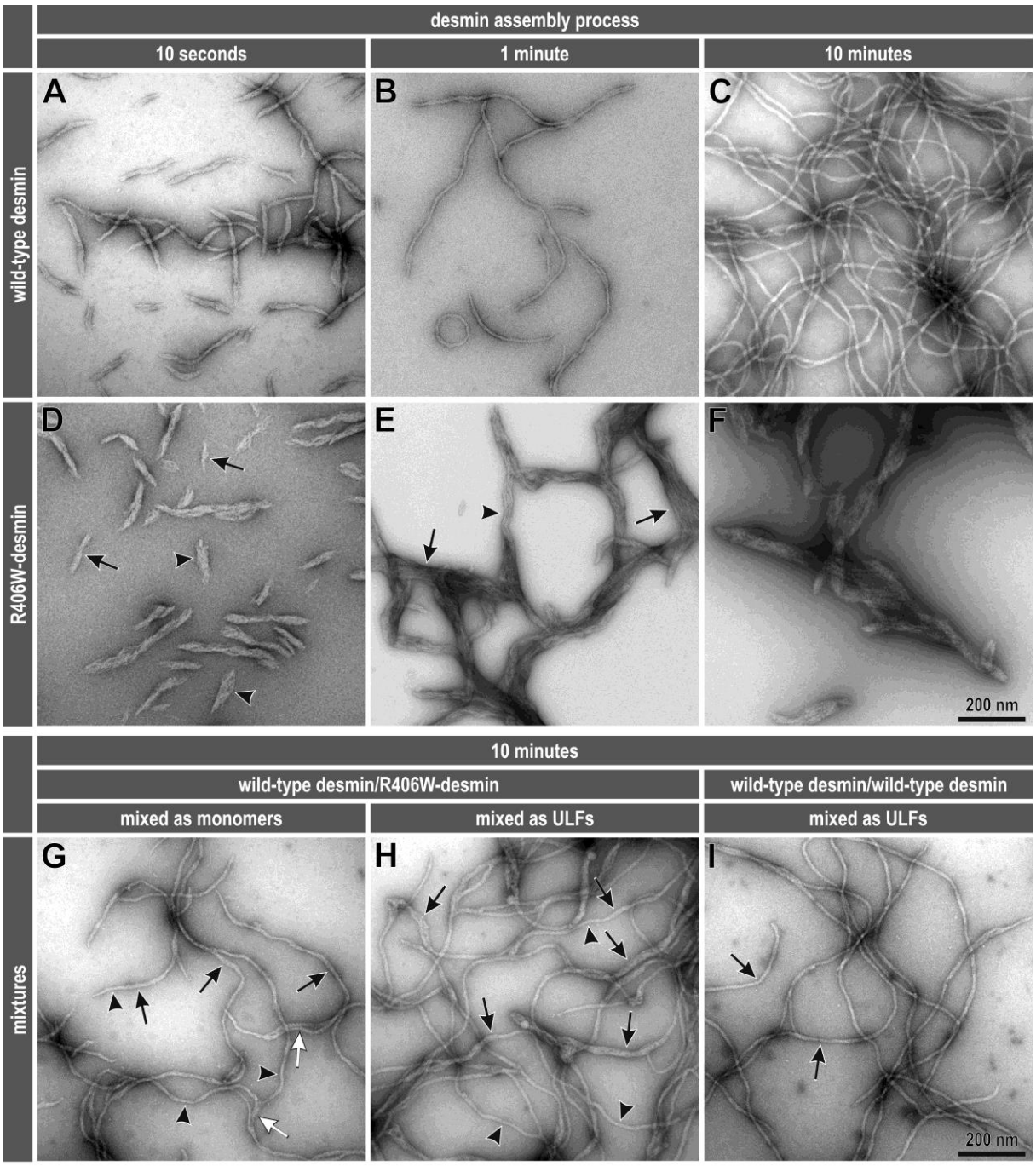
desmin assembly process
10 seconds
1 minute
10 minutes
wild-type desmin
A
B
C
R406W-desmin
D
E
F
200 nm
10 minutes
wild-type desmin/R406W-desmin
wild-type desmin/wild-type desmin
mixed as monomers
mixed as ULFs
mixed as ULFs
mixtures
G
H
I
200 nm

Figure 4

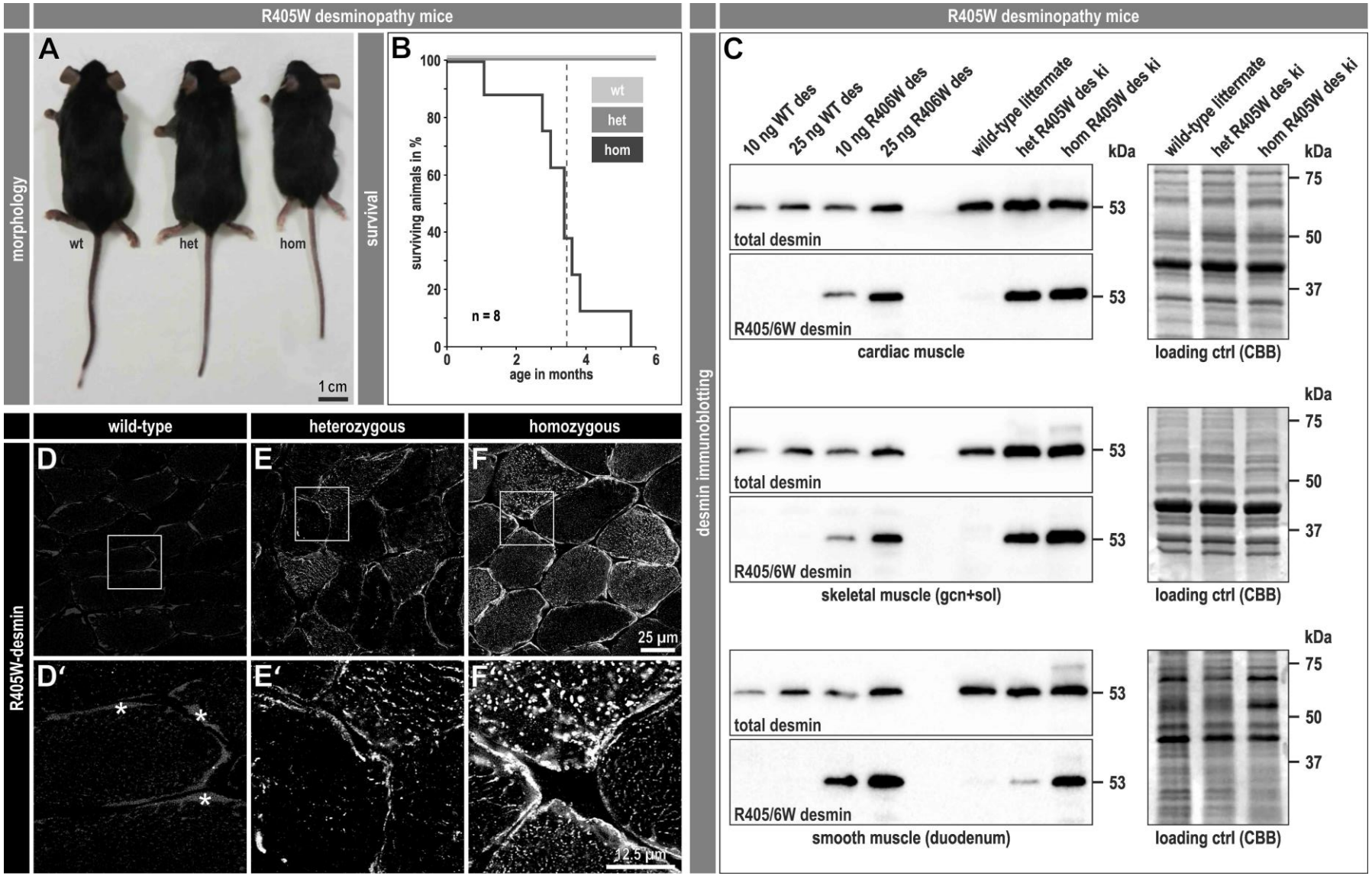
R405W desminopathy mice
morphology
A
wt
het
hom
1 cm
survival
B
surviving animals in %
age in months
n = 8
wt
het
hom
wild-type
heterozygous
homozygous
R405W-desmin
D
E
F
25 µm
D'
E'
F'
12.5 µm
R405W desminopathy mice
desmin immunoblotting
C
10 ng WT des
25 ng WT des
10 ng R406W des
25 ng R406W des
wild-type littermate
het R405W des ki
hom R405W des ki
kDa
total desmin
R405/6W desmin
cardiac muscle
skeletal muscle (gcn+sol)
smooth muscle (duodenum)
loading ctrl (CBB)
53
75
50
37

Figure 5

wild-type
heterozygous
homozygous
desmin (wild-type + mutant)
DAPI
A
A'
B
B'
C
C'
10 µm
5 µm
desmin (wild-type + mutant)
smooth muscle actin
DAPI
wild-type
homozygous
D
E
F
G
H
I
cm
lm
200 µm
200 µm
wild-type
homozygous
desmin (wild-type + mutant)
synaptopodin-2
J
K
L
M
N
O
50 µm
50 µm
transmission electron microscopy
wild-type
homozygous
P
Q
R
S
1 µm
1 µm
1 µm
1 µm

Figure 6

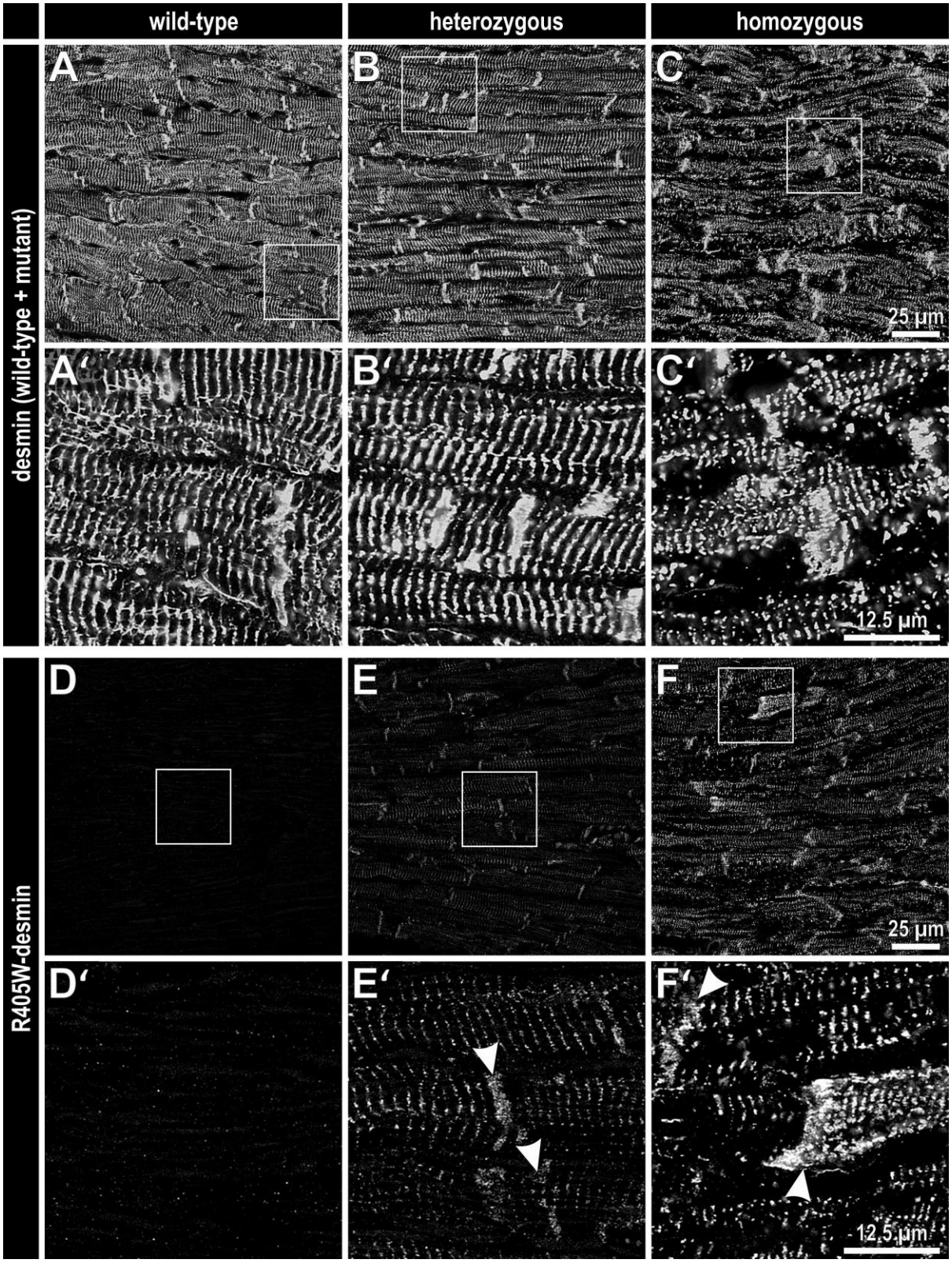

Figure 7

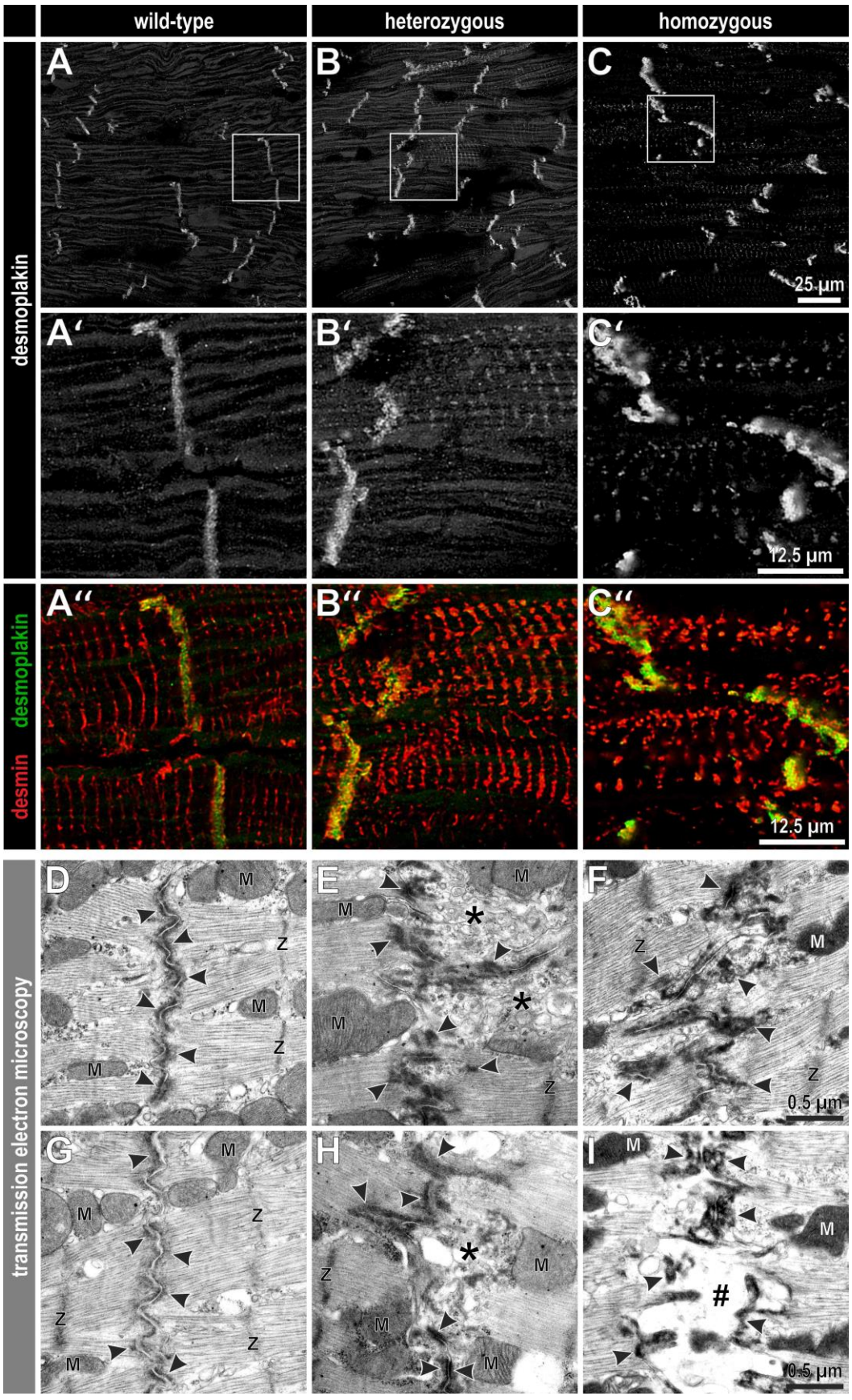
wild-type
heterozygous
homozygous
desmoplakin
A
B
C
25 µm
A'
B'
C'
12.5 µm
desmin
desmoplakin
A''
B''
C''
12.5 µm
transmission electron microscopy
D
E
F
M
Z
*
0.5 µm
G
H
I
#
0.5 µm

Figure 8

SUPPLEMENTAL MATERIAL

Dual functional states of R406W-desmin assembly complexes cause cardiomyopathy with severe intercalated disc derangement in humans and in knock-in mice

Harald Herrmann, PhD[1,2,*,#], Eva Cabet, PhD[3,*], Nicolas R. Chevalier, PhD[4], Julia Moosmann, MD[5], Dorothea Schultheis, PhD[1], Jan Haas, PhD[6], Mirjam Schowalter[1], Carolin Berwanger[7], Veronika Weyerer, MD[8], Abbas Agaimy, MD[8], Benjamin Meder, MD[6,9], Oliver J. Müller, MD[10], Hugo A. Katus, MD[11], Ursula Schlötzer-Schrehardt, PhD[12], Patrick Vicart, PhD[3], Ana Ferreiro, MD[3,13], Sven Dittrich, MD[5], Christoph S. Clemen, MD[7,14,15,§], Alain Lilienbaum, PhD[3,§,#], Rolf Schröder, MD[1,§,#]

1 Institute of Neuropathology, University Hospital Erlangen, Friedrich-Alexander University Erlangen-Nürnberg, Erlangen, Germany
2 B060 - Molecular Genetics, German Cancer Research Center, Heidelberg, Germany
3 Basic and Translational Myology, Unit of Functional and Adaptive Biology, Université de Paris / CNRS UMR 8251, Paris, France
4 Laboratoire Matière et Systèmes Complexes, Université de Paris / CNRS UMR 7057, Paris, France
5 Department Pediatric Cardiology, University Hospital Erlangen, Friedrich-Alexander University Erlangen-Nürnberg, Erlangen, Germany
6 Institute for Cardiomyopathies Heidelberg, Heart Center Heidelberg, University of Heidelberg, Heidelberg, Germany
7 Institute of Aerospace Medicine, German Aerospace Center, Linder Höhe, Cologne, Germany
8 Institute of Pathology, University Hospital Erlangen, Friedrich-Alexander University Erlangen-Nürnberg, Erlangen, Germany
9 Stanford University School of Medicine, Department of Genetics, Stanford, California, USA
10 Internal Medicine III, University Hospital Schleswig-Holstein and University of Kiel, Kiel, and DZHK (German Center for Cardiovascular Research), Partner site Hamburg/Kiel/Lübeck, Kiel, Germany
11 Department of Cardiology, Medical University Hospital Heidelberg, and German Center for Cardiovascular Research, Partner site Heidelberg/Mannheim, Heidelberg, Germany
12 Department of Ophthalmology, University Hospital Erlangen, Friedrich-Alexander University Erlangen-Nürnberg, Erlangen, Germany
13 AP-HP, Reference Center for Neuromuscular Disorders, Pitié-Salpêtrière Hospital, Paris, France
14 Center for Physiology and Pathophysiology, Institute of Vegetative Physiology, Medical Faculty, University of Cologne, Cologne, Germany
15 Center for Biochemistry, Institute of Biochemistry I, Medical Faculty, University of Cologne, Cologne, Germany

[*]These first authors contributed equally to this work.

[§]These senior authors contributed equally to this work.

Running title: R406Wdesmin causes cardiomyopathy in humans & mice

[#]Authors for correspondence:

Harald Herrmann, Institute of Neuropathology, University Hospital Erlangen, Schwabachanlage 6, 91054 Erlangen, Germany; Phone: +49 9131 85 44579; h.herrmann@dkfz-heidelberg.de;

Alain Lilienbaum, Fundamental and Translational Myology Laboratory, Unit of Functional and Adaptive Biology / CNRS UMR8251, Université de Paris, 5 rue Lagroua-Weill Hallé, 75013 Paris, France; Phone: +33 1 57277965; alain.lilienbaum@u-paris.fr

Rolf Schröder, Institute of Neuropathology, University Hospital Erlangen, Schwabachanlage 6, 91054 Erlangen, Germany; Phone: +49 9131 85 34782; rolf.schroeder@uk-erlangen.de

Expanded Materials and Methods

Editorial Policies and Ethical Considerations

Informed consent in writing was obtained from the reported patient. Consultation with the local Ethics committee clarified that the use of the tissue specimens of the patient's explanted heart does not require special approval when used for a single case description. Regarding the cardiac tissue specimens from an anonymous autopsy case used for control, the local Ethics committee stated (reference number 28_19 Bc) that this is in keeping with the German legal regulations.

Clinical investigations

Cardiac catheterization was performed by standard protocol (Axiom Artis; Siemens Medical Solutions, Forchheim, Germany). Under local anesthesia, left femoral vein and femoral artery were cannulated using 6- and 5-French catheters. Pressure and oxygenation measurements were performed in the inferior and superior vena cava, right atrium and right ventricle, pulmonary arteries, aorta, left ventricle, and cardiac output was measured by Swan-Ganz catheter and dopamine stress test was performed. Cardiac magnetic resonance imaging was performed on a 1.5 Tesla magnetic resonance scanner equipped with high-performance gradients (Magnetom Aera; Siemens Healthcare, Erlangen, Germany).

Histology

Routine histology analyses of the human explanted and formalin-fixed heart were performed according to standard protocols.

Murine hearts and soleus muscles were dissected and immediately embedded in tragacanth gum or OCT medium (Fisher Scientific, Illkirch, France), frozen in liquid nitrogen-cooled isopentane, and stored at -80°C. Cryostat sections of 6 µm thickness were collected on microscope slides, air-dried for 30 min, and used for standard histology as well as immunofluorescence analysis.

For analysis of the intestinal tract duodenum, jejunum, ileum, and proximal and distal colon were cut, rinsed with PBS, fixed in formaldehyde prepared from 4% paraformaldehyde at 4°C or in 100% methanol at -20°C, dehydrated in a graded

series of alcohol/water and xylene solutions, and embedded in paraffin. Microtome sections of 6 µm thickness were air-dried for one hour at 60°C, rehydrated, and used for standard histology as well as immunofluorescence analysis.

Generation and genotyping of R405W-desmin knock-in mice

The R405W-desmin knock-in mouse model C57BL/6N-*Des*$^{tm1.1Allb}$ (http://www.informatics.jax.org/allele/MGI:6382607) was generated according to our specifications (AL) by the platform CIPHE (Center for Immunophenomics), Marseille, France. A 760bp cassette harboring the R405W desmin mutation in exon 6 was synthesized by DNA 2.0 (Newark, USA) (Figure IIA in the Supplement). This cassette was cloned into the murine desmin gene in vector "13-22 Des R405W 01 V1", verified, and finally electroporated into C57BL/6N embryonic stem cells. Selected embryonic stem clones were injected into BALB/cN blastulas that were re-implanted into pseudopregnant females. Males displaying more than 50% chimerism were mated with C57BL/6N females, and three independent founders were obtained. Routine genotyping on gDNA from tail biopsies was performed by PCR using the primer pair 5'-CTGGAGGAGGAGATCCGACA-3' and 5'-GGCCCTCGTTAATTTTCTGC-3' (Figure IIB in the Supplement). Presence of the R405W-desmin point mutation was verified by sequencing. Mice were housed in isolated ventilated cages under specific and opportunistic pathogen-free conditions at a standard environment with free access to water and food. Health monitoring was done as recommended by the Federation of European Laboratory Animal Science Associations. Mice were handled in accordance with European Union guidelines and French regulations for animal experimentation, and the investigations were approved by the University Paris Diderot local committee (authorization number CEB-16-2016 / 2016041216476300).

Echocardiography of mice

M-mode echocardiography was performed at the Echography Platform for Small Animals, Cochin Institute, Paris, France, with a Vevo 2100 ultrasound system

equipped with a MS-440D cardiac probe [36]. Mice were kept anesthetized with 1.5% isoflurane during the course of the procedure.

Intestinal force measurement

A 5 cm section of murine duodenum was placed vertically in oxygenated DMEM culture medium at 35°C, and hooked to a flexible glass cantilever to measure longitudinal contraction forces (Movie I in the Supplement). Displacement of the cantilever, calibrated with different weights, was recorded with a camera, and the images were analyzed with ImageJ (NIH, Bethesda, USA). The force signal upper and lower envelopes were computed with the Matlab signal processing routine (Mathworks, Natik, USA). The amplitude of contractions was defined as the time-averaged difference between the upper and lower envelopes.

Stable transfections

The generation of a stable fibroblast line from the vimentin knock-out mouse [19] has been described [37, 38]. We transfected vimentin knock-out cells with the plasmid pHβBAPr-1-neo harboring a β-actin promoter, intron 1 of the human β-actin gene followed by a 5´UTR sequence IVSI linker at the 3'-splice site to a short DNA polylinker segment [39]. The cDNA of human wild-type desmin was cloned into the polylinker sites Sal I and Hind III. The expression plasmid for the R406W mutant was identical except for the mutation in codon 406 of desmin.

Vimentin knock-out cells were seeded at a density of 2.5 x 10^5 cells per 6 cm cell culture dish one day before transfection. The cells were cDNA-transfected with Lipofectamine LTX with PLUS Reagent (Invitrogen, #15338100) according to the manufacturer´s instructions. The final amount of DNA used per 6 cm cell culture dish was 5 µg and the final amount of Lipofectamine LTX Reagent per 6 cm cell culture dish was 15 µl. We employed the constructs pHβBAPr-1-neo-hDesWT and pHβBAPr-1-neo-hDesR406W for transfection. 24 h after transfection 1 mg/ml geneticin was added to the cells to select for successfully transfected cells (the optimal concentration of geneticin was determined prior to this experiment by generating a kill curve). From this point the cells were always cultured in medium containing 1 mg/ml geneticin. In order to allow single cell derived colonies to grow, the cells were diluted 48h after transfection via transferring them from one 6 cm cell culture dish to three 10 cm cell culture dishes. The medium was partially exchanged two

times per week and after two weeks the cell colonies were trypsinized within cloning cylinders and transferred to 12-well plates. For the hDesWT and for the hDesR406W stable transfected cell lines 66 and 92 clones were picked, respectively. Immunofluorescence staining with an antibody directed against desmin was performed with cells from all clones to verify the successful stable transfection and to characterize the cells. To exclude any accidental exchanges of the clones, the immunostaining was performed at least twice for all clones. For each transfected construct at least three different clones were expanded for further analysis.

Transient transfections

3T3 cells or mouse vimentin knock-out fibroblasts were seeded at a density of 1.0 x 10^4, 2.5 x 10^4 and 5.0 x 10^4 cells per well in 6-well plates containing cover slips one day before transfection. The cells were transfected with Lipofectamine LTX with PLUS Reagent (Invitrogen, #15338100) according to manufacturer´s instructions. The final amount of DNA used per 6 cm cell culture dish was 2.5 µg and the final amount of Lipofectamine LTX Reagent per 6 cm cell culture dish was 7.5 µl. pHβBAPr-1-neo-hDesWT and p163/7-hDesR406W were used for the transfections. The plasmid p163/7 uses a human MHC class I H-2-promoter and a 0.5 kb 5'-UTR-β-globin sequence [40]. At 18h, 24h, and 48h after transfection the cells were fixed and stained with antibodies directed against desmin and vimentin.

Immunofluorescence microscopy

Cells were fixed for 6 min in -20°C cold methanol and for 30 s in -20°C cold acetone. Cells were blocked with 1x PBS containing 10% goat serum followed by 30 min incubation with the primary antibodies diluted in 1x PBS containing 10% goat serum. After three 5-minute-long washing steps with 1x PBS, cells were incubated for 30 min with secondary antibodies and DAPI diluted in 1x PBS containing 10% goat serum. After additional three washing steps, 5 min each, with 1x PBS, the cells were first rinsed with distilled water and then with 100% ethanol. After air drying, the coverslips were embedded in Mowiol and stored at 4°C.

Striated muscle tissue sections were fixed for 10 min with acetone at -20°C, and air-dried for 10 min. Non-specific binding was blocked with 10% fetal calf serum, 1% goat serum, and 0.01% sodium azide in PBS for 1 h at room temperature. Smooth muscle sections were blocked in 1% bovine serum albumin in PBS. Incubation with primary antibodies diluted in PBS with 3% BSA was done overnight at 4°C or for 1 h at room temperature. After washing, sections were incubated with secondary antibodies, and finally washed with PBS and mounted in Mowiol.
Microscopic images were acquired with a Zeiss LSM 780 and LSM 700 confocal laser-scanning microscope equipped with the ZEN software (Erlangen and Paris, respectively), and a Leica TCS SP5 confocal laser scanning microscope equipped with HyD detectors and LAS AF software (Cologne). Selected images were deconvolved using Huygens Essential (Jan 2016; Scientific Volume Imaging B.V.) as indicated in the figure legends. Images were processed and figures assembled using Adobe Photoshop CS5 and CorelDraw Graphics Suite X7.

Antibodies

The following primary antibodies were used:

- mouse-anti-desmin (Leica Biosystems, #NCL-L-DES-DERII, dilution 1:100 for immunohistochemistry and immunofluorescence) for detection of total desmin in human tissue specimens

- mouse anti-desmin (DAKO-Thermo Fisher, #M0760, clone D33, dilution 1:100 for immunofluorescence) for detection of total desmin in murine tissue specimens

- rabbit-anti-desmin-CT1 (prepared by immunizing rabbits with the human desmin carboxy-terminal peptide CG-VSEATQQQHEVL coupled to Keyhole limpet hemocyanin; PSL Peptide Speciality Laboratories GmbH, Heidelberg, Germany; sera were affinity-purified on columns with the peptide coupled to sepharose; 1:100 for immunofluorescence, 1:20,000 for immunoblotting) for detection of total human and murine desmin in tissue specimens and cells

- rabbit-anti-R406W-desmin (prepared by immunizing rabbits with the human desmin peptide CG-TYWKLLEGE coupled to Keyhole limpet hemocyanin; PSL Peptide Speciality Laboratories GmbH, Heidelberg, Germany; sera were affinity-

purified on columns with the peptide coupled to sepharose; 1:50 for immunofluorescence, 1:1,000 for immunoblotting) for detection of human R406W and murine R405W-desmin in tissue specimens and cells

- guinea pig-anti-plectin-P2 directed against the carboxy terminal repeat domain 6 of human plectin ([41], 1:250 for immunofluorescence) for detection of plectin in human tissue samples

- guinea pig-anti-desmoplakin-495 (kind gift from W. W. Franke, see [42], available as DP-1 from Progen Biotechnik; for immunofluorescence 1:100 on formalin-fixed paraffin-embedded tissue sections, 1:500 on cryosections) for detection of desmoplakin in human and murine tissue samples

- rabbit-anti-N-cadherin (Abcam, #ab18203, 1:100 for immunofluorescence) for detection of N-cadherin in human tissue samples

- rabbit-anti-connexin-43 (Cell Signaling, #3512S, 1:25 for immunofluorescence) for detection of connexin-43 in human tissue samples

- rabbit-anti-vimentin-CT targeting the last nine carboxy-terminal amino acids (kind gift from Thomas Magin, University of Leipzig, Germany; 1:500 for immunofluorescence) for detection of vimentin in cells

- mouse-anti-vinculin (Sigma-Aldrich, #V9131, 1:300 for immunofluorescence) for detection of vinculin in human tissue specimens

- mouse-anti-smooth muscle actin (Sigma-Aldrich, #202M-9, clone 1A4, dilution 1:100 for immunofluorescence) for detection of smooth muscle actin in murine tissue specimens

- rabbit-anti-synaptopodin-2 (Thermo-Fisher, #PA5-21055, dilution 1:50 for immunofluorescence) for detection of synaptopodin-2 in murine tissue specimens.

The following fluorescence-labelled secondary antibodies were used at a 1:250 dilution: goat anti-mouse AlexaFluor488 (Invitrogen, #A11001), goat anti-mouse AlexaFluor 555 (Invitrogen, #A21424), goat anti-rabbit AlexaFluor488 (Invitrogen, #A11034), donkey anti-rabbit AlexaFluor555 (Invitrogen, #A31572), and goat anti-guinea pig AlexaFluor488 (Invitrogen, #A11073). Nuclei were stained with either DAPI or Hoechst 33258.

Protein biochemical procedures

Recombinant desmin and desmin variants were isolated from *E. coli* essentially as described [43]. Three independent protein preparations were generated for both wild-type desmin and R406W-desmin. Purity and performance of the proteins were checked by SDS-PAGE and analytical ultracentrifugation [20]. For assembly experiments, we used two regimens. The urea-denatured proteins were reconstituted into low ionic strength dialysis buffers consisting either of 2 mM sodium phosphate, pH 7.5, (buffer A) or 5 mM Tris-HCl, pH 8.4, (buffer B) as described [43]. With both buffers, stable tetrameric complexes were obtained. To start assembly, an equal volume of dialysis buffer (A) containing 200 mM potassium chloride was added with gentle agitation to enable immediate mixing (method A). Alternatively, dialysis buffer (B) containing 320 mM sodium chloride was employed (method B). Assembly was at a protein concentration of 0.2 mg/ml at 37°C except in the length distribution measurements, where we employed 0.05 mg/ml. Assembly was stopped by addition of an equal volume of assembly buffer containing 0.2% glutaraldehyde.

Immunoblotting

For the extraction of proteins from muscle tissue, small amounts of snap-frozen tissue specimens were pulverized in a mortar on dry ice before addition of lysis buffer (5 mM Tris, 10% SDS, 0.2 M DTT, 1 mM EDTA, pH 6.8). Samples were boiled at 95°C for 5 min, sonicated for 10 s, again boiled at 95°C, and centrifuged at 13,000 xg for 10 min based on [44, 45]. Supernatants were used undiluted for protein quantitation using a fluorometric dye (ProStain, Active Motif, Carlsbad, CA, USA), and 1:4 diluted with 1x SDS sample buffer (25 mM Tris, 0.8% SDS, 2% 2-mercaptoethanol, 4% glycerol, 0.001% bromophenol blue, pH 6.8) and again boiled for SDS-PAGE and Western blotting. For full transfer of high molecular weight proteins, wet transfer in 10 mM borate, pH 8.8, was performed at constant current with 200 mA overnight followed by another hour at 300 mA the next morning, all at room temperature.

Electron microscopy

In vitro desmin assembly assays: Fixed samples were deposited onto carbon-coated grids, stained with uranyl-acetate and imaged in transmission mode with a Zeiss 900 or 912 electron microscope (Carl Zeiss, Oberkochen, Germany) as described [43].

Cardiac and soleus muscle specimens: Samples were fixed in 2.5% glutaraldehyde in 0.1 M phosphate buffer, pH 7.2, post-fixed in 2% buffered osmium tetroxide, dehydrated in graded alcohol concentrations, and embedded in epoxy resin according to standard protocols. 1 µm semi-thin sections for orientation were stained with toluidine blue. Ultra-thin sections were stained with uranyl acetate and lead citrate, and examined with a LEO 906E transmission electron microscope (Carl Zeiss GmbH, Oberkochen, Germany).

Duodenum tissue specimens: Samples were fixed in 2% glutaraldehyde, post-fixed in 1% osmium tetroxide, and embedded in Araldite M (Sigma-Aldrich). Ultrathin sections were counterstained with uranyl acetate and lead citrate, and examined using a JEOL 1011 transmission electron microscope at the Electron Microscopy Platform, Cochin Institute, Paris, France.

Statistical analysis

For statistical evaluation the non-parametric test function “nparcomp” of the free software R was used with Dunnet comparison to wild-type, Tukey comparison for others, or the Kruskal-Wallis test. Differences were considered significant with $p<0.05$.

Expanded Results

The assembly process of wild-type and mutant desmin protein species

Like all intermediate filament proteins, the desmin protein is fibrous in nature and exhibits a tripartite structure with a central α-helical coiled-coil domain ("rod") flanked by non-α-helical "head" and "tail" domains (for details of the assembly process see [28]). Driven by its intrinsic self-assembly properties, the multistep formation of the three-dimensional desmin filament network starts with the dimerization of two desmin molecules by coiled-coil formation of their central α-helical rod domains. Two such desmin dimers associate into a half-staggered, antiparallel tetramer (Figure IA in the Supplement). Tetramers are the essential *in vitro* building elements for the spontaneous assembly of 60 nm-long filaments (Figure IA in the Supplement), which are the principal units for intermediate filament formation. Therefore, they have been termed *unit-length filaments* or ULFs. The further formation of the extended intermediate filament network is driven by longitudinal annealing of ULFs with each other and successively of short filaments. Elongated desmin filaments spontaneously reduce their diameter by radial compaction from 17 to 14 nm during the first 10 min of assembly and eventually form stable mature desmin intermediate filament [46].

The assembly behavior of individual desmin disease mutants is complex, as some of them form long filaments whereas others do not assemble beyond the ULF-state, as we previously revealed by investigating recombinant proteins of fourteen different desmin mutants [20, 30]. In particular, we demonstrated that these individual mutant proteins deviated at specific points from the assembly pathway originally described for the general assembly pathway of cytoplasmic intermediate filament proteins using vimentin and desmin as model proteins [46-48]. The first group of desmin mutants already failed to form the first assembly product, that is ULF; the second group formed ULF but failed to longitudinally anneal, so that their assembly stopped at this stage; the third group did elongate, however, at a certain length, filaments aggregated laterally indicating that the radial compaction was not executed but instead an unproductive lateral association took over; the fourth group formed seemingly normal intermediate filament but did not perform normal during strain experiments [30, 49] (Figure IA in the Supplement). Specifically, the R406W-desmin mutant was originally grouped into category 2, because assembly products observed by electron microscopy were mainly ULFs with the presence of some short

filaments [30]. According to the new findings, we would group this mutant into an extra category reflecting the dual behavior, i.e., its ability at physiological ionic strength for normal elongation in combination with simultaneous enhanced lateral association reflecting two possible folding states of the tetrameric complexes.

In vitro assembly confirms the dual behavior of the R406W mutant desmin protein

The clinical results obtained here with the patient exhibiting multiple small aggregates in cardiomyocytes prompted us to have a closer look at the assembly properties of R406W-desmin to get an idea what kind of structures the subunits of the *in vivo* aggregates could relate to.

Originally, in order to directly compare a larger number of different desmin mutants by viscometry, we assembled proteins at comparatively low ionic strength conditions of 25 mM Tris-HCl (pH 7.5) with 50 mM sodium chloride [20], because at higher salt concentrations desmin tended to clog the viscometer capillaries during measurements. To challenge the R406W-desmin with an ionic strength closer to physiological ionic strength conditions, we changed the assembly medium to 2 mM sodium phosphate (pH 7.5) with 100 mM potassium chloride. Here, we observed that at one second of assembly, R406W-desmin formed ULFs similar in appearance to those assembled from wild-type desmin, exhibiting already double, triple and higher ULF-containing filaments (Figure IB,C in the Supplement). However, the width-control of R406W-desmin appeared to be impaired compared to wild-type desmin as filaments of R406W-desmin often exhibited a larger diameter (Figure IC, arrows, in the Supplement).

In order to get insight into the assembly kinetics of both proteins during the first 30 s of assembly, we measured their length development over time by electron microscopy as has previously been implemented for the quantitative description of vimentin assembly [50]. In comparison to the experiments presented in Figure IB,C in the Supplement, we lowered the protein concentration fourfold in order to capture ULFs and first elongation products, before they would laterally aggregate to a significant extent. Under these conditions, the assembly kinetics of R406W-desmin were very similar to those of wild-type desmin (Figure ID,E in the Supplement). At

10 s, the distribution of the filament length revealed approximately 69% of the intermediate filaments to be ULFs, around 22% consisted of two ULFs and 7% of three ULFs, compared to 57%, 31% and 5% exhibited by wild-type desmin, respectively. At 30 s, however, R406W-desmin did not show the continued productive elongation as exhibited by wild-type desmin, mostly due to substantial lateral aggregation of growing filaments, which also impeded accurate length measurements.

Irregular composite filament formation from mutant and wild-type desmin

The trend of the mutant protein to assemble into filaments with larger diameter was also kept in composite filaments of mutated and wild-type protein, when we mixed R406W-desmin and wild-type desmin in various ratios, either when they were still monomers, i.e., in 8 M urea, or after their reconstitution into tetramers, i.e., in low ionic strength buffer with no salt. Hence, although the mutant and wild-type proteins were compatible for co-assembly, the mutant dominantly imposed the formation of partly unraveled filaments in contrast to more compact filaments as exhibited by the wild-type protein in the early stages of assembly (data not shown).

To explore if tetramers, containing both R406W-desmin and wild-type desmin in equal amounts, can assemble into extended filaments after longer times of assembly or if they would predominantly aggregate, we followed their assembly for up to 10 min. Notably, filaments were not as smooth and flexible as those formed by wild-type desmin, often exhibiting kinks and segments with irregular morphology (Figure 4G, arrows). However, aggregates were hardly observed under these conditions. As the mutant protein did not cause major aggregation, we assume that the presence of the wild-type protein apparently rescued in part the unproductive interactions during the lateral assembly reaction. Nevertheless, due to the random distribution of R406W-desmin and wild-type desmin to dimers and tetramers during renaturation from urea, ULF-segments with varying subunit composition are generated. But as longer segments with normal diameter and flexibility were present in individual filaments (Figure 4G, arrowheads), we assume a kinetic sort-out of ULFs with higher percentage of wild-type molecules may occur during elongation to some extent. In addition, on occasion individual filaments appeared to have laterally fused

(Figure 4G, white arrows). Moreover, whereas the wild-type desmin filaments do significantly radially compact from 1 to 10 min (Figure 4B,C; see also [46]), the mixed mutant desmin filaments did not reorganize consistently but kept the more irregular and wider diameter most probably representing R406W-desmin rich ULF segments.

In a next step, we investigated the assembly process of a composite system of mutant and wild-type desmin at the ULF-short filament stage. We started the assembly of both proteins separately, mixed them after 10 s of assembly, and carried out assembly for further 10 min. The mixed R406W-desmin and wild-type desmin filaments were distinctly heterogeneous exhibiting thick segments, originating from R406W-desmin filaments (Figure 4H, arrows), and segments of normal diameter apparently originating from wild-type desmin filaments (Figure 4H, arrowheads). Nevertheless, wild-type desmin filaments had apparently fused end-on to the mutant filaments recapitulating the hetero-filament formation observed in 3T3 cells (Figure 3B-B'''). For control, wild-type desmin subjected to this procedure formed typical intermediate filaments of uniform diameter, on occasion revealing points where individual segments had annealed (Figure 4I, arrows). Hence, the assembly was not significantly disturbed by the mechanical interference potentially introduced when the two assembling protein samples were combined after 10 s of assembly. Actually, at this time point filaments enter an intense elongation and reorganization process.

Assembly studies under physiological sodium chloride conditions

We have previously shown for vimentin that intermediate filaments with similar properties are obtained when assembled in the phosphate-KCl versus the Tris-NaCl system, though some differences were observed in the way the proteins reacted to the specific salt condition such as the diameter of the filaments formed. We further noted that both vimentin and desmin reacted sensitive to the absolute ionic strength in that they assemble faster with increasing salt concentration. As a consequence of the fast assembly, we observed enhanced entanglement of long filaments, and therefore we employed a lower salt concentration for desmin in capillary viscometer experiments [20]. Guided by this observation, we assembled both R406W-desmin and wild-type desmin in the Tris-NaCl system to investigate how the mutant desmin is

affected when the salt concentration is raised into the physiological range, i.e., 160 mM NaCl. To prepare for assembly experiments in this system, monomeric proteins are renatured as usual by dialysis from 8 M urea into 5 mM Tris-HCl, pH 8.4 (dialysis buffer), which yields uniform tetrameric species [20]. Assembly is "jump-started" by addition of buffered salt solution such that a final setting of 25 mM Tris, pH 7.5, 160 mM NaCl is obtained. After 10 s of assembly, R406W-desmin filaments exhibited a significantly higher degree of open conformation compared to wild-type desmin ULFs and filaments (Figure 4A,D). Note that for the mutant desmin, ULFs with low diameter (Figure 4D, arrows) were found in addition to the large diameter assemblies (Figure 4D, arrowheads). Thus, during early lateral assembly competing interactions take place leading to ULFs with different numbers of subunits per cross-section. This kind of polymorphism is also found with wild-type desmin to some degree, although it stays within a range of 32 to 48 monomers per cross-section [46]. In particular, the maturation phase characterized by a radial compaction of the filament diameter is still observed with wild-type desmin [28].

In order to gain more insight into the next higher order, i.e., an intermediate stage of fibrillar substructure organization of the mutant protein assemblies, we performed high-resolution imaging after 60 s of assembly under these ionic conditions (Figure 4E). Mutant fibers had grown large by intense inter-fibril association, both longitudinally and laterally. Band-like associations had apparently wrapped around each other, just engaging into further wraps after a few 100 nm with further strands (Figure 4E, arrowhead). Eventually, the length of individual fiber strands could not be followed anymore because fiber strands had entangled further into composite structures including sheet-like arrays with small regions of quasi-paracrystalline organization (Figure 4E, arrows). This behavior of R406W-desmin fibers is in stark contrast to that of wild-type desmin filaments, as the latter only longitudinally anneal thus entirely carrying out proper filament elongation. As example for the regularity of assembly, the image depicts single wild-type desmin filaments (Figure 4B). In addition, we occasionally observed wild-type desmin filaments that had closed into a circle. This peculiar structural arrangement again highlights desmin's principal high intrinsic flexibility and the propensity of desmin filaments to faithfully longitudinally elongate without undergoing unproductive interactions. However, even in crowded areas desmin filaments did not aggregate but formed complex networks (Figure 4C). After 10 min, elongation of filaments appeared to have come to an end for R406W-

desmin. Instead, a significant increase of lateral association of the polymers had occurred, some of the composite fiber arrays showing diameters of more than 30 nm (Figure 4F).

Solubility properties of mutant and wild-type desmin do not differ

In standard assembly experiments, we found that all of the R406W-desmin was recovered in pellets after centrifugation in a conventional benchtop centrifuge for 10 min (15,000 x g), thus sedimenting like wild-type protein (Figure IF in the Supplement). As ULFs and short intermediate filaments do not pellet under these conditions, we concluded that the R406W-desmin filaments and filamentous aggregates formed are indeed large enough to sediment under these low centrifugation forces. In order to investigate if such aggregates formed are trapped in potentially irreversibly misfolded structures such as indicated above (Figure 4E), we subjected the pelleted material to conditions dissolving wild-type intermediate filament (5 mM Tris-HCl, pH 8.4, *dialysis buffer*) [47]. Notably, both wild-type desmin and R406W-desmin were nearly completely recovered in the supernatant already after 15 min mild agitation. After slightly longer incubation of the pellets in dialysis buffer, not even a trace of protein was recovered in the pellet in both cases (data not shown). This simple and straight forward experiment demonstrates that both R406W-desmin and wild-type desmin are soluble after brief incubation under low ionic strength conditions and that no irreversibly aggregated, amyloid-type material had formed that would need more harsh solvents to dissolve (Figure IG in the Supplement).

Homozygous R405W-desmin knock-in mice die from smooth muscle-related intestinal pseudo-obstruction

At birth, homozygous mice had the same body weight and size as heterozygous and wild-type littermates. However, within the first three months of life homozygous mice developed significantly reduced values for body weight and size (Figure IIC,D in the Supplement). Moreover, they displayed reduced motor activity, a prostrated posture, a swollen abdomen, and increased lethality (Figure 5B). Abdominal echography

revealed a severe gut dilatation limited to the small intestine in homozygous but not heterozygous mice (data not shown). This was also a very prominent feature upon dissection of homozygous mice which disclosed a swollen, liquid and air-filled duodenum and jejunum (Figure IVA-C, upper part, in the Supplement). Further macroscopic analysis demonstrated that the total length of the gastrointestinal tract was reduced by 30% in homozygous mice as compared to wild-type animals (Figure IVA-C, lower part, in the Supplement; Figure VB in the Supplement), while its diameter was increased by 80% and 30% in sections of the duodenum and colon, respectively (Figure VB, right part, in the Supplement). These findings strongly indicate a severe intestinal motility defect similar to chronic intestinal pseudo-obstruction in humans.

Microscopic analysis of H&E stained gut tissue sections (Figure IVD-I in the Supplement) showed an altered villus morphology in the duodenum, jejunum, and ileum of homozygous mice, in which the epithelial layer seemed to be detached from the underlying mesenchymal cells (Figure IVF in the Supplement). Further H&E image evaluation revealed an increased thickness of both the longitudinal and circular layers of the muscularis propria from the ileum (Figure VC in the Supplement). This was accompanied by an increased nuclear density in the muscular layers of ileum and colon from homozygous mice, whereas there was a decrease in the duodenum and jejunum (Figure VC in the Supplement).

Finally, we addressed the contractile properties of the digestive tract (Figure VA in the Supplement; Movie I in the Supplement). While the spontaneous pendular oscillations frequencies of the duodenal segments were within a similar range, with values of 0.53 ± 0.02 Hz for wild-type, 0.54 ± 0.01 Hz for heterozygous, and 0.53 ± 0.02 Hz for homozygous mice, the mean amplitude of spontaneous contractions in duodenum from homozygous mice was reduced to 34% of the wild-type level (Figure VA,B in the Supplement). Stimulation with 1 µM carbachol, a stable agonist of the acetylcholine receptor inducing a force increase, resulted in a markedly attenuated effect in the duodenum of homozygous mice (Figure VA,B in the Supplement). Taken together, our findings demonstrate that the sole expression of R405W-desmin leads to structural and functional defects in intestinal smooth muscle tissue resulting in a lethal pseudo-obstruction phenotype.

Expanded Discussion

A molecular “wobble”-segment in mutated desmin coil 2: a key to the dual structural state of mutant protein complexes

The amino acid segment surrounding arginine 406 in desmin is highly conserved in the evolution of the intermediate filament protein family [27], and when mammalian intermediate filament protein sequences are compared, this arginine is hardly ever replaced by another amino acid. Even in nuclear intermediate filament proteins of invertebrates such as *Hydra* lamin, this arginine is found as part of a conserved 20 amino acid stretch. Indeed, it is conserved together with a glutamic acid at position 401 five amino acids upstream of this arginine. Both amino acids are completely charged under physiological conditions and form an inter-helical salt bridge between the two chains of the coiled-coil dimer as revealed in the first crystallized intermediate filament protein fragment covering this segment [27]. This end domain of the coiled coil is resistant to attempts to mechanically open it as demonstrated by single-molecule force spectroscopy using optical tweezers [51]. Hence, this salt bridge may stabilize and orient the coiled coil before the two chains open up and fold away from the axis of the coiled coil, by means of the highly negatively charged segment Glu-Gly-Glu-Glu. Immediate neighboring amino acids are, however, of great importance for regular assembly, too, and the sequence is indeed conserved over a large stretch between desmin and vimentin [52]. Thus, when the equivalent of desmin tyrosine 405 in vimentin, i.e., tyrosine 401, is mutated to leucine or serine, vimentin’s filament assembly is entirely arrested at the ULF stage [29].

In contrast, the mutation R406W in desmin does not impede the elongation reaction at all, but with respect to the lateral assembly exhibits more open and, depending on the ionic conditions, band-like ribbons and sheets (see Figure 4E). Therefore, one may assume that the very much stabilized end segment is now, with the arginine to tryptophan mutation, less decisive but instead wobbles between different structural states, functioning as a molecular oscillator segment. How would this impact filament formation? At the mechanistic level of filament elongation, it is two dimers of two ULFs each that directly interact in an overlap mode, i.e., it is an interaction between the carboxyl-terminal end of one dimer with the amino-terminal end of the dimer of two connecting ULFs. Thereby, 16 dimers of every ULF, eight with their amino-terminus and eight with their carboxyl-terminus, interact successively to the second

ULF to connect to a full intermediate filament segment (see Figure IA in the Supplement, for the orientation of the dimers in the tetramer, which is retained in the ULF). The essential molecular interaction of two dimers has been demonstrated with the nuclear intermediate filament proteins lamin A and lamin B, which are the primordial intermediate filament proteins from which the cytoplasmic intermediate filament proteins have been evolved [53]. Depending on the ionic conditions, lamin dimers will associate in a “head-to-tail” manner, such that the amino-terminal ends of the rod domain of one dimer functionally engage in an overlap-type interaction with the carboxy-terminus of a second dimer. This overlap occupies a segment of 3 nm equivalent to a stretch of 21 nm in the coiled coil. As we demonstrated in this study, not only the longitudinal annealing interaction but also the kinetics of filament elongation is not changed for the mutant. We know that this domain is very dynamic at the molecular level, as revealed by hydrogen-deuterium exchange analysis [29]. Therefore, we speculate that the loss of salt bridge formation by introduction of the tryptophan, presenting a voluminous side chain compared to that of arginine, leads to alternative steric conformations at this strategic site of the dimer ends that allow normal ULF formation but also additional lateral associations as indicated by the occurrence of normal as well as wide and open ULF in parallel (Figure IA in the Supplement, Figure 4E).

Despite the fact that these less organized tetramers can engage into new, mainly lateral interactions leading to extended sheets, the structures obtained are easily dissolved under low ionic strength conditions indicating that they do not contain severely misfolded structures, such as amyloid or “pre-amyloid” fibers. The occurrence of such material has previously reported to be generated upon desmin phosphorylation [54]. Correspondingly, we did not obtain staining of R406W aggregates with Congo Red, which would trace amyloidic proteins, in tissue sections from the patient’s heart (data not shown).

The control of dimer formation

Since the conserved short end-segments of the rod domain are instrumental for the elongation reaction, it is no surprise that they are so highly conserved in evolution. Obviously because of this nearly complete sequence identity, ULFs and longer

filaments of desmin and vimentin are able to longitudinal anneal and form a composite filament [48]. In principle, due to the very high sequence identity of both proteins, one could argue that vimentin represents a desmin mutated at multiple sites, except for large parts of the rod domain, as demonstrated by a comprehensive sequence analysis over various species from shark to man [52]. Moreover, most of the changes seen are homologous, therefore a change from arginine to tryptophan as manifested in the R406W mutant is a rather drastic change. So, when structurally and functionally similar intermediate filament proteins such as desmin and vimentin are mixed at the monomeric stage, they can form heterodimers and further mixed tetramers and correspondingly heterogeneous ULFs [55, 56]. An analogous reaction to this *in vitro* mixing would be a co-translational assembly mechanism in the cell.

At present, we do not know how coiled-coil formation is organized in the living cell and to what extent segregation may occur. However, both chemical crosslinking [55] and immunofluorescence microscopy (see for instance Figure 3A,B) indicate that mixed desmin and vimentin filaments are present in cells. In contrast, a strict segregation in cells has been found for the desmin mutant R350P from wild-type desmin filaments [17]. In line with this principle, nuclear intermediate filament proteins lamin A and lamin C, which are different splice forms from one gene and which are identical over the entire α-helical rod, do segregate completely [30, 57]. The cellular mechanisms operating in this segregation, in particular the way how the different protein forms are recognized, are not known yet. Proteolytic targeting appears not to be a relevant mechanism, as in heterozygous R349P desmin knock-in mice similar amounts of both the wild-type and the mutant protein are present, and therefore an enhanced degradation of the mutant to prevent integration into desmin intermediate filament is not taking place [45]. In contrast, R406W-desmin forms in fibroblasts separate structures but at the same time also integrates into filaments (Figure 3B,D). Very much the same in skeletal muscle of the patient, R406W-desmin appears to partly segregate into aggregates and to integrate into desmin-containing structures. On its own, R406W-desmin does not form extended filaments in cells that lack desmin and vimentin but instead only granular structures, very similar to the *in vitro* situation at physiological sodium chloride concentration where the mutant hyper-aggregates, in stark contrast to the wild-type protein (Figure 4A-F). Hence, it is likely that the mutant gets chaperoned when it is in a molecular complex with the wild-type

protein. And this in turn makes the mutant dangerous for the desmin system as it introduces new and non-productive properties of the mutant into the chimeric filaments. From these filaments a molecular pathology originates by providing interacting complexes and organelles with a “floppy” hub, thus undermining the continued establishment of a functional myocyte cell architecture.

Taken together, our *in vitro* assembly work showed that a molecular defect in one of the domains of desmin, which is operational for both lateral association and elongation, introduces a structural “uncertainty element” for assembly that is at the center of the development of a malignant cardiomyopathy.

Supplemental Figure Legends

Supplemental Figure I

Assembly properties of desmin and R406W-desmin. (**A**) Schematic diagram highlighting the principal phases of the filament assembly process for desmin and the points of deviation from the standard assembly pathway as exhibited by desmin mutants [1]. Tetrameric complexes, made from half-staggered anti-parallel dimers, are induced to assemble by increase of the ionic strength. Phase 1: the first assembly products are unit-length filaments (ULFs). Phase 2: ULFs longitudinally anneal to short filaments, which further elongate by interacting with ULFs and other short filaments. Phase 3: filaments stabilize by radial compaction, which for desmin results in a reduction of the filament diameter from 17 to 14 nm as measured at 10 s and 10 min of assembly [46]. According to the assembly properties of mutant desmin variants, their cellular appearance and distribution may vary considerably from that of wild-type desmin filaments. (**B**,**C**) The assembly of wild-type desmin and R406W-desmin was started by addition of salt and immediately stopped after one second by addition of glutaraldehyde to 0.1%. Protein concentration, 0.2 mg/ml. Elongation kinetics of wild-type desmin (**D**) compared to R406W-desmin (**E**) for 10 s and 30 s. Protein concentration, 0.05 mg/ml. Abscissa, filament length expressed in multiples of the ULF-unit segment repeat length within filaments (43 nm). Ordinate, percentage of filaments with the indicated length. For every time point >100 filaments were measured. (**F**) Filamentous structures obtained by assembly for 1 h (in, input sample) were centrifuged in a tabletop centrifuge. Aliquots from supernatant (sn) and pelleted (p) fractions were processed for gel electrophoresis. (**G**) Solubility of R406W-desmin fibrillar aggregates compared to wild-type desmin filaments in low salt “tetramer” buffer. In, renatured protein in “tetramer” buffer; fil-s, filament solution after 1 h of incubation with assembly buffer; sn1, supernatant of filament solution after centrifugation; the filament pellet was resuspended in “tetramer” buffer, incubated for 15 min and then spun in a tabletop centrifuge at top speed; sn2, supernatant; p2, corresponding pellet.

Supplemental Figure II

Generation and phenotyping of the R405W-desmin knock-in mice. (**A**) Schematic drawing of the gene targeting strategy. The nine exons of the desmin gene are represented by boxes filled in light blue; open boxes represent untranslated regions. A fragment of exon 6 (red box) harboring the c.1213C>T mutant codon was synthesized and cloned to the 5'-end of a neomycin cassette (neo) flanked by LoxP sites. Below, a schematic drawing of the desmin protein domain structure is given; the red box represents the amino acid region encoded by exon 6. (**B**) PCR-genotyping of wild-type, heterozygous, and homozygous mice showed the expected 370 bp amplicon derived from the mutant allele, which still contains one remaining LoxP sequence in intron 6 after Cre-mediated excision of the neomycin cassette, and the 285 bp product from the wild-type allele. +, equimolar mixture of wild-type and R405W-desmin constructs was used as template for positive control; –, no template as negative control. (**C**) Column chart of the mean body sizes of wild-type, heterozygous, and homozygous mice. Error bars represent standard errors of the mean. (**D**) Body weight development of desminopathy mice and wild-type siblings. At the age of three months, homozygous males have significantly reduced body weights, whereas females showed a tendency towards weight reduction. Mean values and standard errors are shown.

Supplemental Figure III

Echocardiography of R405W-desmin knock-in mice. (**A**) Echocardiographic investigation of wild-type, heterozygous, and homozygous desminopathy mice aged one, three, and eighteen months. Notably, younger homozygous mice showed a significantly higher left ventricular ejection fraction and a lower PAT/PET ratio (pulmonary acceleration time to pulmonary ejection time ratio) as compared to wild-type mice (values highlighted in grey). Aged heterozygous mice, however, exhibited significantly lower values of left ventricular diastolic volume and diameter as well as an increased systolic interventricular septum thickness (values highlighted in grey).

Supplemental Figure IV

Macroscopic and microscopic analysis of the intestinal phenotype in R405W desminopathy mice. (**A**-**C**) Macroscopic view of the abdominal cavity (upper images) and the isolated gastrointestinal tract (lower images) of three-months-old mice. Homozygous mice display markedly dilated duodenums and jejunums with accumulation of liquid and gas. Moreover, they displayed a marked shortening of the entire gastrointestinal tract (Figure VB, right part, in the Supplement). E, esophagus; S, stomach; D, duodenum; J, jejunum; I, ileum; A, appendix; C, colon; R, rectum. H&E stained gut tissue sections of duodenum (**D**-**F**) and colon (**G**-**I**) depicted an altered villus morphology in the duodenum as well as an increased thickness of the muscularis propria of the colon in homozygous animals. Arrowheads, detachment of the epithelial layer from the underlying connective tissue.

Supplemental Figure V

Contractile properties of the duodenum in R405W-desminopathy mice. (**A**) Measurement of the contractile activity of the duodenum from three-month-old wild-type and homozygous mice. The characteristic recording depicted a deficiency in the oscillating duodenal contractile activity of homozygous mice both at the basal state and after cholinergic stimulation (carbachol) as compared to the wild-type. (**B**) Mean force amplitudes developed by duodenums from homozygous desminopathy mice are significantly lower as compared to wild-type siblings (values highlighted in grey). Moreover, the length of the total intestine from duodenum to rectum as well as the diameters of duodenum and colon were markedly reduced in homozygous mice (values highlighted in grey). (**C**) The muscularis propria of the ileum was thicker in homozygous than in wild-type mice and showed an increased density of nuclei in the ileum and colon and a decreased density in the duodenum and jejunum (values highlighted in grey). The number of nuclei in 600 μm^2 delimited surfaces in smooth muscles was counted for each segment of the intestine.

Supplemental Movie I

Comparative view of spontaneous gut movements of 5 cm duodenal sections from a wild-type sibling (wt, left movie) and a homozygous R405W desmin knock-in mouse (hom, right movie).

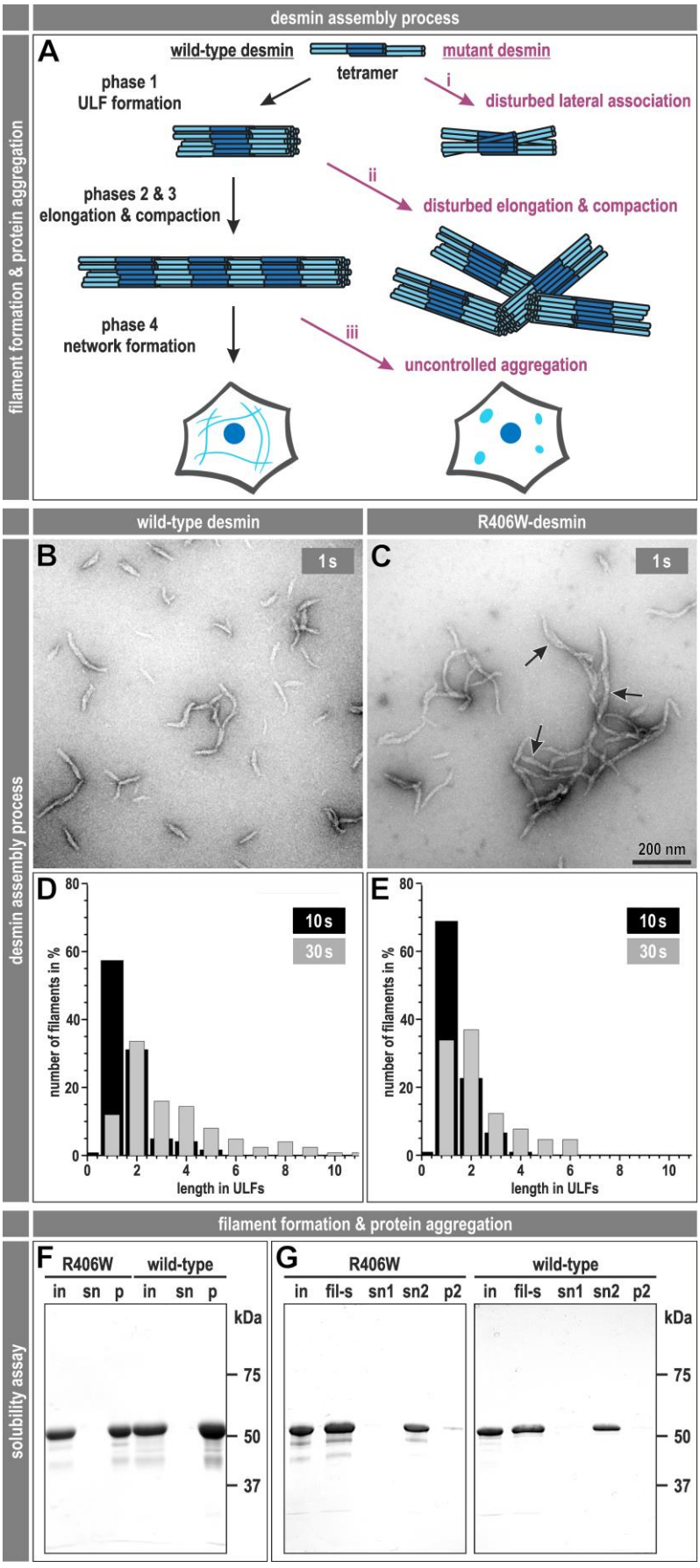

Supplemental Figure I

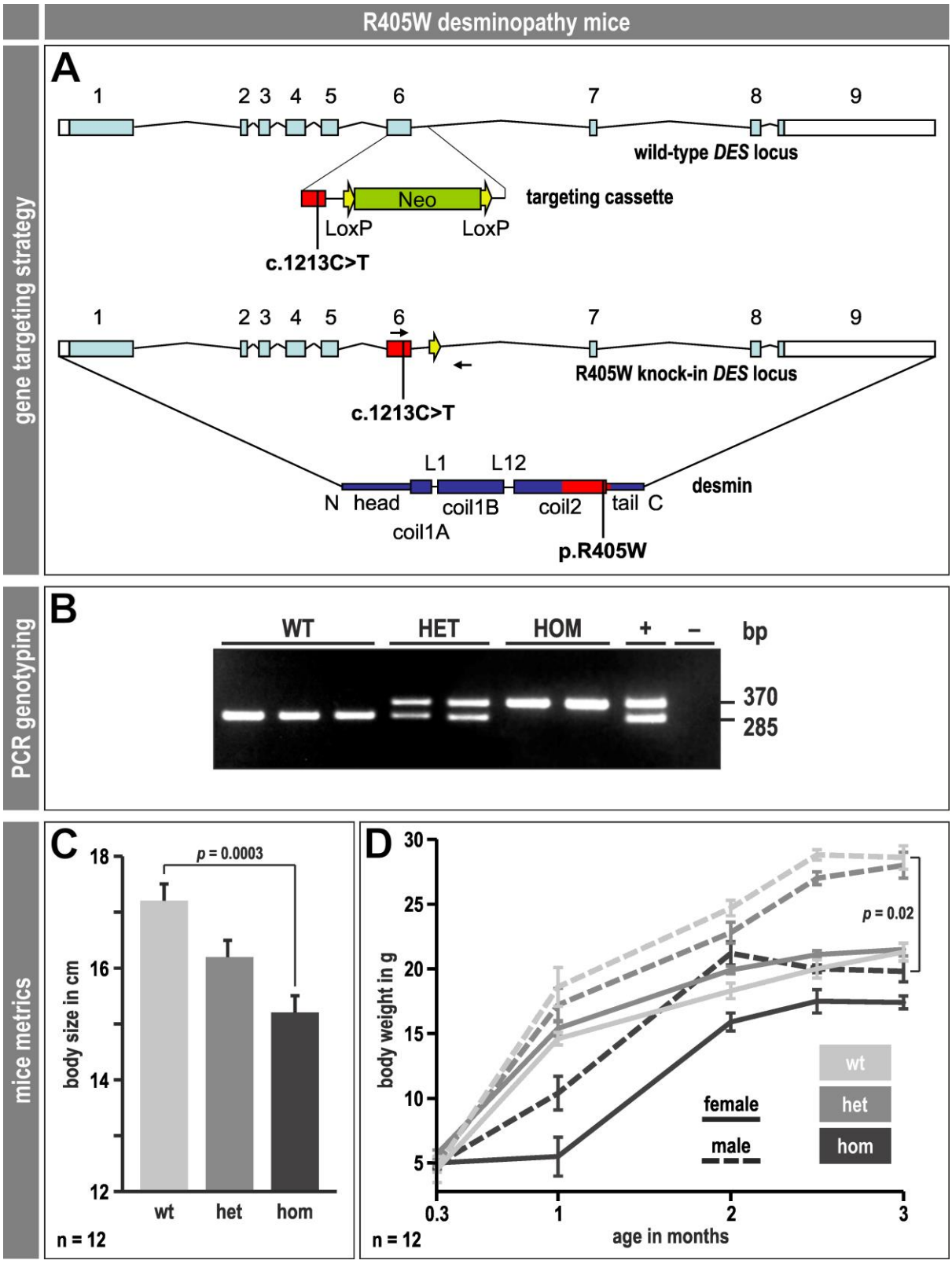

Supplemental Figure II

Supplemental Figure III

R405W desminopathy mice

echocardiography

A	Left ventricular ejection fraction	Left ventricular enddiastolic volume	Diastolic left ventricular internal diameter	Diastolic left ventricular posterior wall	Systolic inter-ventricular septum	Diastolic inter-ventricular septum	E wave velocity	A wave velocity	E/A ratio	Isovolumic relaxation time	PAT/PET ratio
	%	µL	mm	mm	mm	mm	mm/s	mm/s		ms	
no. of 1 months old animals	6	6	6	6	6	6	6	6	6	6	6
WT (1 month)	53 ± 3	57.1 ± 2.9	3.67 ± 0.08	0.76 ± 0.08	0.91 ± 0.03	0.67 ± 0.03	787 ± 58	536 ± 74	1.52 ± 0.10	13.3 ± 1.4	0.31 ± 0.01
HET (1 month)	56 ± 3	68.1 ± 3.6	3.95 ± 0.09	0.65 ± 0.04	0.99 ± 0.02	0.72 ± 0.02	839 ± 29	535 ± 32	1.59 ± 0.08	12.9 ± 0.8	0.30 ± 0.02
HOM (1 month)	68 ± 2	47.0 ± 2.8	3.38 ± 0.08	0.69 ± 0.07	0.99 ± 0.05	0.71 ± 0.03	853 ± 43	500 ± 24	1.71 ± 0.05	14.8 ± 1.5	0.25 ± 0.01
p (HET vs. WT)	0.94	0.18	0.18	0.59	0.32	0.63	0.78	0.48	0.93	0.97	0.89
p (HOM vs. WT)	0.02	0.40	0.40	0.69	0.30	0.76	0.65	0.93	0.36	0.77	0.03
no. of 3 months old animals	6	6	6	6	6	6	6	6	6	6	6
WT (3 month)	41 ± 1	82.7 ± 5.5	4.28 ± 0.12	0.73 ± 0.13	0.95 ± 0.03	0.72 ± 0.01	861 ± 37	483 ± 38	1.81 ± 0.13	18.1 ± 1.3	0.36 ± 0.02
HET (3 month)	40 ± 2	84.9 ± 4.5	4.33 ± 0.10	0.61 ± 0.03	0.92 ± 0.04	0.75 ± 0.04	804 ± 56	517 ± 27	1.55 ± 0.07	23.2 ± 1.8	0.29 ± 0.03
HOM (3 month)	59 ± 4	68.8 ± 4.4	3.97 ± 0.11	0.68 ± 0.09	0.98 ± 0.15	0.79 ± 0.09	737 ± 66	493 ± 44	1.50 ± 0.02	17.2 ± 1.2	0.23 ± 0.03
p (HET vs. WT)	0.99	0.96	0.96	0.65	0.79	0.96	0.70	0.78	0.38	0.10	0.34
p (HOM vs. WT)	0.10	0.31	0.31	0.98	0.89	0.84	0.29	0.95	0.09	1.00	0.02
no. of 18 months old animals	3	3	3	3	3	3	3	3	3	3	3
WT (18 month)	48 ± 3	102.5 ± 2.0	4.70 ± 0.04	0.85 ± 0.06	1.07 ± 0.01	0.87 ± 0.03	643 ± 41	478 ± 134	1.60 ± 0.49	16.1 ± 0.6	0.31 ± 0.03
HET (18 month)	55 ± 3	83.6 ± 4.5	4.31 ± 0.10	0.97 ± 0.05	1.27 ± 0.09	1.02 ± 0.08	748 ± 19	660 ± 9	1.13 ± 0.04	15.4 ± 1.3	0.32 ± 0.03
p (HET vs. WT)	0.13	0.05	0.05	0.28	0.05	0.13	0.08	0.56	0.56	1.00	0.83

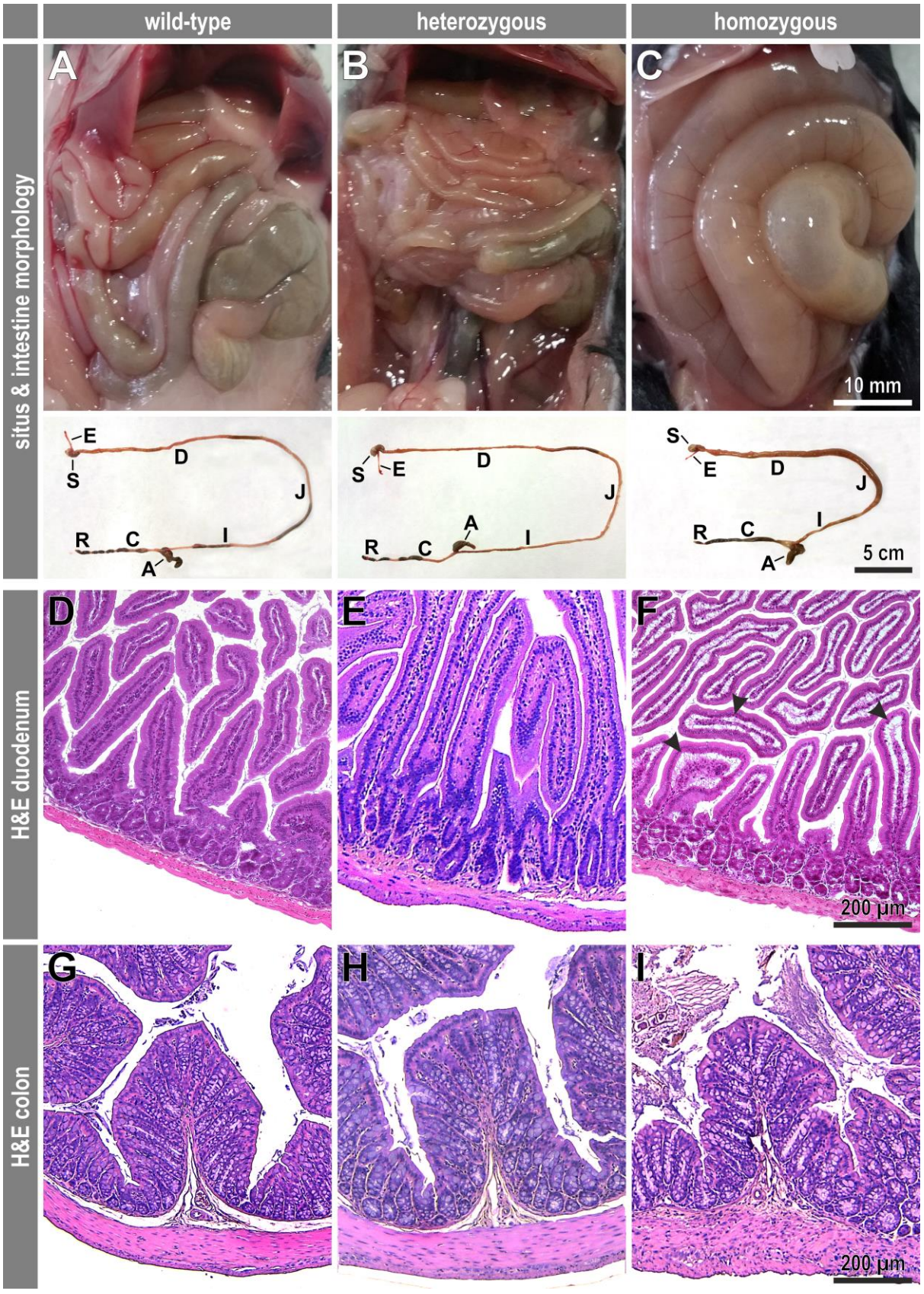

Supplemental Figure IV

R405W desminopathy mice

duodenum contractility

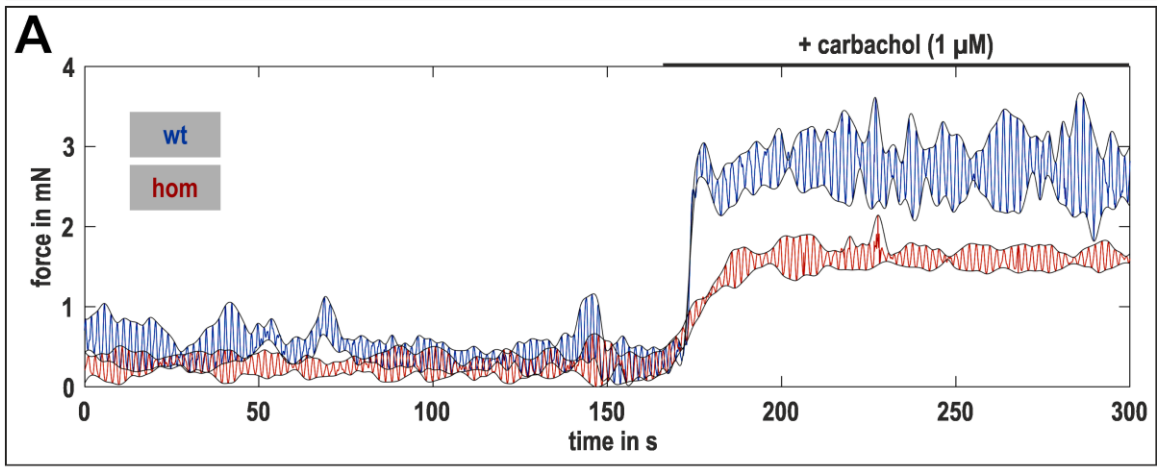

force & morphology

B

	force w/o carbachol (amplitude)	force with carbachol (amplitude)	force development (Δforce)	length of intestine	length/weight ratio	diameter of duodenum	diameter of colon
	mN	mN	mN	cm	cm/g	mm	mm
no. of 3 months old animals	4	4	4	4	4	4	4
WT	0.54 ± 0.15	0.60 ± 0.05	2.04 ± 0.12	44.8 ± 0.8	1.9 ± 0.1	1.4 ± 0.1	1.6 ± 0.1
HET	0.46 ± 0.13	0.48 ± 0.09	1.47 ± 0.18	45.7 ± 0.6	1.8 ± 0.1	1.5 ± 0.2	2.2 ± 0.1
HOM	0.15 ± 0.07	0.18 ± 0.05	0.96 ± 0.31	33.1 ± 1.4	1.8 ± 0.1	2.6 ± 0.2	2.2 ± 0.1
p (HET vs. WT)	1.00	0.98	0.57	1.00	1.00	1.00	0.04
p (HOM vs. WT)	0.05	0.01	0.06	0.01	1.00	0.04	0.08

muscularis propria

C

	duodenum	jejunum	ileum	proximal colon	distal colon	duodenum	jejunum	ileum	proximal colon	distal colon
	muscularis propria thickness in µm					muscularis propria nuclei per 100 µm²				
no. of 3 months old animals	4	4	4	4	4	4	4	4	4	4
WT	45.3 ± 6.4	33.5 ± 5.4	60.7 ± 2.7	84.9 ± 7.1	74.4 ± 7.2	111.4 ± 7.6	103.0 ± 3.7	75.0 ± 4.8	83.8 ± 3.8	71.8 ± 5.3
HET	41.1 ± 3.3	30.5 ± 2.8	58.2 ± 5.1	78.9 ± 6.6	61.0 ± 5.5	80.0 ± 4.5	84.3 ± 3.2	130.3 ± 7.0	156.5 ± 6.4	139.7 ± 1.0
HOM	41.5 ± 1.4	36.0 ± 1.7	115.9 ± 3.5	142.8 ± 6.7	130.8 ± 7.2	65.3 ± 1.3	63.7 ± 0.9	168.0 ± 3.3	171.5 ± 1.4	155.5 ± 5.5
p (HET vs. WT)	1.00	1.00	1.00	1.00	1.00	0.51	0.42	0.35	0.19	0.32
p (HOM vs. WT)	1.00	0.98	0.06	0.12	0.17	0.01	0.01	0.01	0.01	0.01

Supplemental Figure V